A new assessment of global and regional budgets, fluxes and lifetimes of atmospheric reactive N and S gases and aerosols

Yao Ge[1,2], Massimo Vieno[2], David S. Stevenson[3], Peter Wind[4], Mathew R. Heal[1]

[1] School of Chemistry, University of Edinburgh, Joseph Black Building, David Brewster Road, Edinburgh, EH9 3FJ, UK
[2] UK Centre for Ecology & Hydrology, Bush Estate, Penicuik, Midlothian, EH26 0QB, UK
[3] School of GeoSciences, University of Edinburgh, Crew Building, Alexander Crum Brown Road, Edinburgh, EH9 3FF, UK
[4] The Norwegian Meteorological Institute, Henrik Mohns Plass 1, 0313, Oslo, Norway

Correspondence to: Yao Ge (Y.Ge-7@sms.ed.ac.uk), Mathew R. Heal (M.Heal@ed.ac.uk)

Abstract. We used the EMEP MSC-W model version 4.34 coupled with WRF model version 4.2.2 meteorology to undertake a present-day (2015) global and regional quantification of the concentrations, deposition, budgets, and lifetimes of atmospheric reactive N (N_r) and S (S_r) species. These are quantities that cannot be derived from measurements alone. In areas with high levels of reduced N_r (RDN = NH_3 + NH_4^+), oxidised N_r (OXN = NO_x + HNO_3 + HONO + N_2O_5 + NO_3^- + Other OXN species), and oxidised S_r (OXS = SO_2 + SO_4^{2-}), RDN is predominantly in the form of NH_3 (NH_4^+ typically <20%), OXN has majority gaseous species composition, and OXS predominantly comprises SO_4^{2-} except near major SO_2 sources. Most continental regions are now 'ammonia rich', and more so than previously, which indicates that whilst reducing NH_3 emissions will decrease RDN concentration it will have small effect on mitigating SIA. South Asia is the most ammonia-rich region. Coastal areas around East Asia, northern Europe, and north-eastern United States are 'nitrate rich' where NH_4NO_3 formation is limited by NH_3. These locations experience transport of OXN from the adjacent continent and/or direct shipping emissions of NO_x but NH_3 concentrations are lower. The least populated continental areas and most marine areas are 'sulfate rich.' Deposition of OXN (57.9 TgN yr^{-1}, 51%) and RDN (55.5 TgN yr^{-1}, 49%) contribute almost equally to total nitrogen deposition. OXS deposition is 50.5 TgS yr^{-1}. Globally, wet and dry deposition contribute similarly to RDN deposition; for OXN and OXS, wet deposition contributes slightly more. Dry deposition of NH_3 is the largest contributor to RDN deposition in most regions except for Rest of Asia and marine areas where NH_3 emissions are small and RDN deposition is mainly determined by transport and rainout of NH_4^+ (rather than rainout of gaseous NH_3). Reductions in NH_3 would thus efficiently reduce the deposition of RDN in most continental regions. The two largest contributors to OXN deposition in all regions are HNO_3 and coarse NO_3^- (via both wet and dry deposition). The deposition of fine NO_3^- is only important over East Asia. The tropospheric burden of RDN is 0.75 TgN of which NH_3 and NH_4^+ comprise 32% (0.24 TgN; lifetime = 1.6 days) and 68% (0.51 TgN; lifetime = 8.9 days), respectively. The lifetime of RDN (4.9-5.2 days) is shorter than that of OXN (7.6-7.7 days), consistent with a total OXN burden (1.20 TgN) almost double that of RDN. The tropospheric burden of OXS is 0.78 TgS with a lifetime of 5.6-5.9 days. Total nitrate burden is 0.58 TgN with fine NO_3^- only constituting 10% of this total, although fine NO_3^- dominates in eastern China, Europe, and eastern North America. It is important to account for contributions of coarse nitrate to global nitrate budgets. Lifetimes of RDN, OXN, and OXS species vary by a factor of 4 across different continental regions. In East Asia, lifetimes for RDN (2.9-3.0 days), OXN (3.9-4.5 days), and OXS (3.4-3.7 days) are short, whereas lifetimes in Rest of Asia and Africa are about twice as long. South Asia is the largest net exporter of RDN (2.21 TgN yr^{-1}, 29% of its annual emission), followed by Euro_Medi region. Despite having the largest RDN emissions and deposition, East Asia has only small net export and is therefore largely responsible for its own RDN pollution. Africa is the largest net exporter of OXN (1.92 TgN yr^{-1}, 22%), followed by Euro_Medi (1.61 TgN yr^{-1}, 26%). Considerable marine anthropogenic N_r and S_r pollution is revealed by the large net import of RDN, OXN and OXS to these areas. Our work demonstrates the substantial regional variation in N_r and S_r

budgets and the need for modelling to simulate the chemical and meteorological linkages underpinning atmospheric responses to precursor emissions.

1 Introduction

Reactive N (N_r) and S (S_r) gases and particle species are critical determinants of air quality. The principal precursor gas emissions of NO and NO_2 (collectively NO_x), NH_3 and SO_2 are emitted from a wide range of human activities (Crippa et al., 2018; Hoesly et al., 2018). As the dominant alkaline gas in the atmosphere, NH_3 exerts significant control on the acidity of deposition and on the formation of the secondary inorganic aerosol (SIA) components of fine particles ($PM_{2.5}$) (Sutton et al., 2020). The latter derive from the reactions between NH_3 and the sulfuric acid (H_2SO_4) and nitric acid (HNO_3) that are oxidation products of SO_2 and NO_x (Xue et al., 2011; Behera et al., 2013a; Nenes et al., 2020). These particles have significant impacts on human health (Lelieveld et al., 2015; Cohen et al., 2017; Burnett et al., 2018) and on Earth's radiation budget (Bellouin et al., 2011; IPCC, 2021). Sulfur dioxide and sulfate aerosols (collectively referred to as oxidised S and abbreviated as OXS) also have an impact on cloud formation and the acidity of precipitation (Myhre et al., 2017; Aas et al., 2019; Thornhill et al., 2021; McHale et al., 2021).

In addition, oxidised N gases and aerosols such as NO_x, HNO_3, NO_3^-, etc. (collectively abbreviated as OXN), and reduced N gases and aerosol (NH_3 and NH_4^+, collectively abbreviated as RDN), act as powerful plant and microorganism nutrients when deposited to aquatic and terrestrial ecosystems. Excessive anthropogenic input of N can lead to exceedance of N critical loads, which in turn can lead to eutrophication and loss of ecosystem productivity and biodiversity (Erisman et al., 2005; Fowler et al., 2013; Sun et al., 2017). The increase in food production to support a burgeoning human population is increasing agricultural emissions of NH_3 globally, in contrast to the globally declining emissions of SO_2 and NO_x (Fowler et al., 2020). A further factor contributing to the different trend in NH_3 emissions is the lack of regulations in most countries specifically targeted at reducing NH_3 emissions. The relative proportions of the N_r and S_r gas and aerosol species in the atmospheric burdens and wet and dry deposition of RDN, OXN and OXS vary substantially around the world because of the different magnitudes of precursor emissions and local meteorology. Knowledge of how these burdens and depositions vary regionally is important for understanding local impacts and mitigation actions.

This information can be derived from atmospheric chemistry transport models. An advantage of these models is that they can simulate concentrations and depositions of air pollutants at greater spatial and temporal resolution and coverage than can be achieved through ambient measurements. Furthermore, since these models simulate the underlying physical-chemical processes, they allow insight into the chemical and meteorological linkages between emissions, concentrations and deposition of pollutants that measurements cannot reveal: for example, horizontal and vertical pollutant transport, and the proportion of reduced nitrogen in precipitation that derives from rainout of gaseous NH_3 or particulate NH_4^+. A number of global-scale modelling studies of atmospheric N_r and S_r have been undertaken previously. Lamarque et al. (2013) presented a multi-model ensemble of N and S deposition from 1850 to 2100, derived from the Atmospheric Chemistry and Climate Model Intercomparison Project (ACCMIP). The ACCMIP results for 'present day' (year 2000 ACCMIP time slice) showed a multi-model mean deposition of 110 TgN yr^{-1}, and 83 TgS yr^{-1}. Hauglustaine et al. (2014) reported that 'present-day' (2000) fine nitrate and ammonium particles make important contributions to aerosol burdens and direct radiative forcing. Bian et al. (2017) conducted an evaluation of global NO_3^- aerosol in 2008 from 9 models involved in the Aerosol Comparisons between Observations and Models (AeroCom) phase III and reported a large diversity in global tropospheric burdens of HNO_3, NO_3^-, NH_3 and NH_4^+ between the models. Tan et al. (2018) calculated the global S and N deposition in 2010 utilizing results of 11 models from the second phase of the Task Force on Hemispheric Transport of Air Pollution (HTAP II). The results showed that global S and N depositions in 2010 were 84 TgS yr^{-1} and 123 TgN yr^{-1}, respectively. Comparisons of their results with

those from HTAP I indicated that global distributions of S and N deposition had changed considerably between 2001 and 2010. Globally there was a reduction in S deposition of 2 TgS (3%) during this period, with significant reductions in S deposition in Europe, North America, and Russia. In contrast, global N deposition increased by 7 TgN (6%), particularly in South Asia, East Asia, and Southeast Asia. Ackerman et al. (2019) used the GEOS-Chem Chemical Transport Model to estimate global inorganic N deposition from 1984 to 2016 and found an 8% increase from 86.6 to 93.6 TgN yr^{-1}.

These previous modelling studies provide an outlook on the distribution of sulfate-ammonium-nitrate aerosols in the early 2000s with predominant focus on S and oxidised N. However, a more up-to-date examination of the global state of N_r and S_r deposition, atmospheric burden, deposition and lifetime is needed, particularly of the reduced N_r species NH_3 and NH_4^+, which has not previously been comprehensively conducted. In recent years there have been large changes in global and regional NH_3, NO_x and SO_x emissions, especially over South Asia, East Asia, Europe, and North America (Crippa et al., 2018; Hoesly et al., 2018). For instance, Kurokawa and Ohara (2020) reported that emissions of SO_2 and NO_x in East Asia increased rapidly from 1950 to 2015, reaching their peaks during 2005-2015, yet NH_3 emissions continued to increase. On the other hand, NO_x and SO_2 emissions in South Asia have continued to increase between 1996 and 2015 (Sadavarte and Venkataraman, 2014; Pandey et al., 2014; Kurokawa and Ohara, 2020). In Europe and the United States there has been a general decreasing trend of N and S emissions is in the last decade (Westervelt et al., 2017; UNECE, 2020; Westervelt et al., 2021).

An updated global modelling of N_r and S_r gases and aerosols with the latest available emission inventory is crucial to understand current differences in gas-aerosol partitioning, wet and dry deposition, tropospheric burden and lifetime of separate RDN, OXN, and OXS species in separate regions, and as a basis for developing mitigation strategies according to regional conditions. In this study, we use the three-dimensional global EMEP MSC-W model 4.34 coupled with WRF 4.2.2 meteorology to calculate the atmospheric concentration, deposition, and tropospheric budget of N_r and S_r gases and aerosols in 2015. Section 2 details the framework of our model simulation including emission, meteorology, and aerosol scheme. The global distribution and typical magnitude of N_r and S_r concentration, regional deposition processes of RDN (NH_3, NH_4^+), OXN (NO_x, HNO_3, HONO, N_2O_5, fine NO_3^-, coarse NO_3^-, other OXN species) and OXS (SO_2, SO_4^{2-}), tropospheric budgets and lifetimes of major N_r and S_r species are described in Sect. 3. We summarise the conclusions of our study in Sect. 4.

2 Methods

2.1 Model description

We used version rv4.34 of the EMEP MSC-W (European Monitoring and Evaluation Programme Meteorological Synthesizing Centre –West) open-source atmospheric chemistry transport model (www.emep.int), which is widely used in scientific research and policy development (Simpson et al., 2012; Bergström et al., 2012; Bergström et al., 2014; Jonson et al., 2017; Karl et al., 2019; McFiggans et al., 2019; Fagerli et al., 2019; Pommier et al., 2020). The model was driven by meteorology from the Weather Research and Forecast model (WRF; www.wrf-model.org; https://github.com/wrf-model/WRF/releases/tag/v4.2.2) version 4.2.2 at 1° grid resolution (Vieno et al., 2010, 2014, 2016; Gu et al., 2021). The WRF simulation in this work assimilates data of the numerical weather prediction model meteorological reanalysis from the US National Center for Environmental Prediction (NCEP)/National Center for Atmospheric Research (NCAR) Global Forecast System (GFS) (Saha et al., 2010). The global EMEP-WRF configurations are detailed in Ge et al. (2021).

A detailed technical description of EMEP MSC-W rv4.0 is documented in Simpson et al. (2012). An overview of model updates from version rv4.0 to rv4.34 is presented in Simpson et al (2020). The model has horizontal resolution of 1° × 1° and contains 21 terrain-following vertical layers from the surface to 100 hPa. The lowest model layer has height ~50 m and surface concentrations of most species were adjusted to correspond to 3 m above the surface as described in Simpson et al. (2012; 2020).

Deleted:

Formatted: No underline

Moved down [1]: Ge et al.

Deleted: (2021) document a comprehensive evaluation of surface concentrations and wet deposition of N_r and S_r species from this model configuration against global measurements.

The model aerosol scheme is the Equilibrium Simplified Aerosol Model V4 (EQSAM4clim) (Metzger et al. 2012; 2016; 2018), which efficiently parameterises the aerosol water uptake and full gas-liquid-solid partitioning of mixtures of semi-volatile and non-volatile compounds. In addition to the SO_4^{2-}-NO_3^--NH_4^+ scheme, the model includes the reactions between HNO_3 and dust and sea salt to produce coarse nitrate. The aerosol scheme is described in more detail in Supplementary Material Sect. S1.1.

Dry deposition of gaseous species is simulated utilizing deposition velocity as described in Simpson et al. (2012; 2020). Aerosol dry deposition follows similar formulation to other studies (Lamaud, 1994; Gallagher et al., 1997; Nemitz et al., 2004), with modification for nitrogen compounds (Petroff et al., 2008b, a; Simpson et al., 2012). For wet deposition, all generic fine particles (e.g., SO_4^{2-}, NH_4^+, NO_3^-_f, etc.) have the same wet scavenging ratio (in-cloud) and size-dependent collection efficiency of aerosols by raindrops (below-cloud), whilst coarse particles are divided into two groups (coarse sea salt and other coarse particles) with their own sets of parameters (Berge and Jakobsen, 1998; Laakso et al., 2003; Simpson et al., 2012).

2.2 Emissions

Anthropogenic emissions were derived from V6 of the ECLIPSE (Evaluating the CLimate and Air Quality ImPacts of Short-livEd Pollutant) emission inventory (https://iiasa.ac.at/web/home/research/researchPrograms/air/ECLIPSEv6.html). This contains global annual emissions for 2015 of SO_2, NO_2, NH_3, CO, CH_4, NMVOC (non-methane volatile organic compounds), primary $PM_{2.5}$ and primary coarse particulate matter (PM_{co}) (Klimont et al., 2017) at a horizontal resolution of 0.5°. All emissions were aggregated to 1° resolution internally in the model. The ECLIPSE emission sector-layers were re-assigned to 11 Selected Nomenclature for sources of Air Pollution (SNAP) sectors (Ge et al., 2021). Monthly emission profiles by country/region and by emission sector based on EDGAR (Emission Database for Global Atmospheric Research, v4.3.2 datasets) time series (Crippa et al., 2020) (https://edgar.jrc.ec.europa.eu/dataset_temp_profile) were then applied to the ECLIPSE annual emissions for each pollutant. The calculation of the time-splitting factors for a given pollutant and country/region is given in Ge et al. (2021). The terminology $ECLIPSE_E$ is used here to refer to these monthly emissions.

Dimethyl sulphide (DMS), lightning NO_x, soil NO_x and isoprene emissions were configured as reported in Simpson et al. (2017; 2020) as were the wind-derived emissions of sea salt particles and dust (Tsyro et al., 2011; Simpson et al., 2012). Emissions from forest and vegetation fires, and international shipping were also included.

2.3 Model performance

Formatted: Font colour: Auto

Moved (insertion) [1]

Ge et al. (2021) provide a comprehensive evaluation of surface concentrations and wet deposition of N_r and S_r species from this model configuration against global measurements from 10 monitoring networks. Comparisons of 2010 and 2015 surface concentrations between model and measurement demonstrate that the model captures well the overall spatial and seasonal variations of the major inorganic pollutants NH_3, NO_2, SO_2, HNO_3, NH_4^+, NO_3^-, SO_4^{2-}, and their wet deposition in East Asia, Southeast Asia, Europe, and North America. Correlation coefficients between modelled and measured annual mean concentrations of all species are >0.78 except for HNO_3 and SO_2, and are 0.78 and 0.63 for annual wet deposition of reduced N and oxidised N, respectively. Given the intrinsic scale mismatch between a local site measurement and a global-scale chemistry model grid, these comparisons are good, and are comparable with model evaluation statistics determined for models of similar resolution (Hauglustaine et al., 2014; Bellouin et al., 2011; Pringle et al., 2010; Xu and Penner, 2012).

Both model and measurement have uncertainty that constrains the extent to which statistical analyses between modelled and measured data can be utilized to assess a model's performance. Model uncertainty comes from uncertainty in emission and meteorology inputs and from parameterisations of chemical/physical processes, while measurement uncertainty comes from sampling and analytical procedures. Emission inventory compilation is partially based on reported measurement data and partially on expert estimation, which complicates assigning uncertainties to both emission magnitudes and their spatiotemporal

profiles. It is therefore not possible to quantify the contribution of emissions uncertainty to model uncertainty, but it will surely vary regionally and for different species. We have demonstrated in Ge et al. (2021) that modelled concentrations of secondary pollutants are less sensitive to the choice of emission inventory than for primary pollutants since the former are influenced by multiple emissions and the timescales for their formation act to smooth out the differentials in primary emissions. On the other hand, if it is variation in measurement accuracy that contributes to regional variation in model-measurement agreement, then confidence in model output is maintained. Ge et al. (2021) showed better evaluation statistics with measurements in Southeast Asia, Europe, and North America than in East Asia, which suggests shortcomings in regional measurements and/or emissions in the latter network rather than substantial systematic issues with model parameterisations of chemical/physical processes. Ge et al. (2021) also evaluated model response to changes between 2010 and 2015 ECLIPSE$_E$ emissions and showed that modelled concentration changes of primary and secondary pollutants and of deposition of reduced N, oxidised N, and oxidised S, were consistent with the trends in the corresponding measurements, given realistic uncertainties in emissions and measurements and of meteorological influences between the two years.

Nevertheless, considering the fundamental uncertainties in emission, model and measurement, all numbers reported in this work should be considered as having underlying uncertainty, albeit that the latest available emission inventory and model version were used to minimize as far as possible uncertainties from the first two of these.

2.4 Definition of groups of chemical species

The following terminology is used to refer to groups of N_r and S_r species. RDN represents atmospheric reduced N and is the sum of NH_3 and NH_4^+. OXN represents all oxidised N outputs in the model and consists of HNO_3, NO_x, NO_3^-_f, NO_3^-_c and 'Rest_OXN.' The latter comprises N_2O_5, HONO, and 'Other_OXN' species, which is mainly composed of organic oxidised N species, of which the predominant component is PAN (peroxyacetylnitrate). Full details are given in Table S1. Total reactive N is the sum of RDN and OXN. OXS represents oxidised S and is the sum of SO_2 and total SO_4^{2-}.

In this paper, all concentrations, depositions, emissions, and burdens are expressed as mass of the species (e.g., μg m^{-3}, mg m^{-2}) unless otherwise specified (e.g., μgN m^{-3}, μmol m^{-3}, TgN yr^{-1}).

2.5 Definition of world regions

Deleted: 4

To compare atmospheric budgets and deposition of N_r and S_r species around the world, we divide the world into the 10 regions illustrated in Fig. 1 (and listed in Table S2). These are based on the 58 reference land and ocean regions defined by the Intergovernmental Panel on Climate Change (IPCC) (Iturbide et al., 2020), each of which represent consistent regional climate features. The rationale behind their definition, and their homogeneity, are documented in Iturbide et al. (2020). Nine of our regions are continental (albeit with some local surrounding seas); our 'Rest of world' region incorporates the majority of the oceans and the remotest continental areas of Antarctica and Greenland.

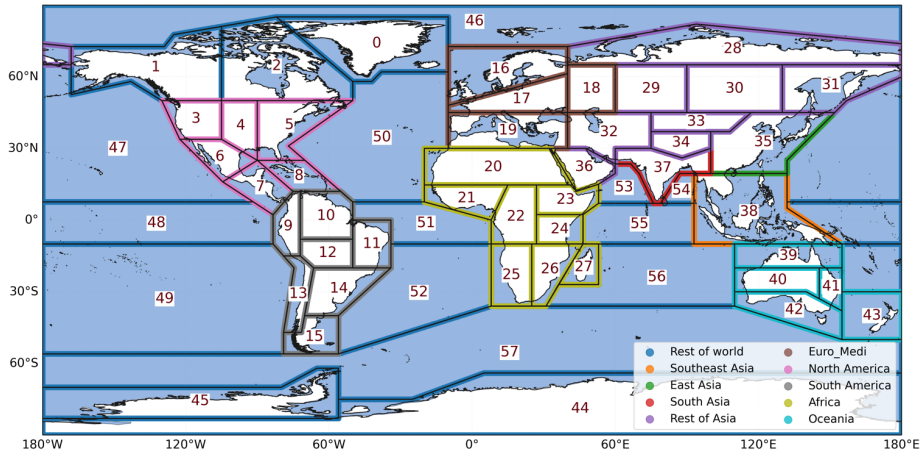

Figure 1: The boundaries of the 10 world regions used in this study, which in turn are based on the IPCC reference regions described in Iturbide et al. (2020).

3 Results and discussion

3.1 Global N_r and S_r concentration distributions

3.1.1 Surface distributions

Figure 2 shows the annual mean surface concentrations of RDN, OXN and OXS and the proportions of each of these that are in the aerosol phase. Maximum concentrations of RDN, OXN and OXS are observed over the continental regions, particularly eastern China and northern India. These are the regions with largest population densities and emissions of NH_3, NO_x and SO_x, as shown in Ge et al. (2021). The surface distributions of these N_r and S_r species are broadly consistent with previous global modelling studies using GEOS-Chem (Zhu et al., 2015), STOCHEM-CRI (Khan et al., 2020), LMDz-INCA (Hauglustaine et al., 2014) and IMPACT (Xu and Penner, 2012).

The maximum RDN concentrations reach 39 μgN m^{-3} in eastern China, 27 μgN m^{-3} in northern India, 19 μgN m^{-3} in southern Europe, and 7-12 μgN m^{-3} in eastern United States, south-eastern South America, and eastern Africa. Fertilizer application and livestock farming contribute most to NH_3 emissions in East Asia, South Asia, Europe, and North America, while biomass burning plays an important role in NH_3 emissions in central and eastern Africa (Aksoyoglu et al., 2020; Bray et al., 2018; Dammers et al., 2019; Wang et al., 2018; Whitburn et al., 2015). All these regions combine both high concentrations of RDN and small proportions of NH_4^+ (typically <20%). Gaseous NH_3 therefore dominates RDN, indicating that whist reducing NH_3 emissions over these regions will effectively decrease total RDN concentrations it will have little effect on mitigating SIA formation. A clear increasing gradient of NH_4^+ fraction from around 20% to ~80% is observed away from these hotspots indicating conversion of NH_3 to NH_4^+ as it disperses from emission sources. The longer lifetime and consequent longer travel distance of NH_4^+ compared with NH_3 (see further discussion on this in Sect. 3.3), means that NH_4^+ accounts for over 90% of RDN in remote areas such as over the oceans, deserts, and polar regions.

In general, the concentrations of surface OXN and OXS are also greatest in regions of high RDN concentrations (Fig. 2). This is especially the case over eastern China (maximum: 49 μgN m^{-3} for OXN, 31 μgS m^{-3} for OXS) and northern India (maximum: 33 μgN m^{-3} for OXN, 14 μgS m^{-3} for OXS). The global maximum OXS concentration (54 μgS m^{-3}) surrounds Norilsk in northern Russia where there are very large SO_2 emissions from nickel and palladium mining and smelting operations

(Fioletov et al., 2020). As illustration of the magnitude of the SO_x emission from that single model grid (560 Gg yr^{-1}), it is double the SO_x emission for the whole of the UK (274 Gg yr^{-1}) in 2015.

Over continental regions, OXN is predominantly gaseous (NO_x, HNO_3, HONO, N_2O_5, etc.) in areas with both high and low OXN concentrations apart from the remote arid regions of the Sahara, Arabia, and Tibetan Plateau. The high proportion of gaseous OXN is driven by the widespread emissions of NO_x wherever there is population. In contrast, NO_3^- is the major form of OXN over oceans, aside from the major shipping routes (e.g., the sea route from the southern edge of Africa to Southeast Asia) where there are also abundant NO_x emissions. The general dominance of aerosol OXN over the oceans is driven both by sea-salt particles acting as an important marine source for coarse NO_3^- (Lee et al., 2014; Schwier et al., 2017) and the reduced depositional sink for gaseous OXN giving time for gas to aerosol OXN conversion.

The formation of fine NO_3^- and coarse NO_3^- follows different chemical pathways and therefore their concentrations and spatial distributions are closely associated with the differing availability of their individual precursors. Figure S1 shows that fine NO_3^- predominates within total NO_3^- over eastern China, Europe, eastern North America, and south-eastern South America, reflecting a relative abundance of gaseous NH_3 in these regions. In contrast, coarse NO_3^- accounts for >80% of total nitrate over India, Africa, and most of the oceans, which indicates large sources of coarse particles in these regions. Karydis et al. (2016) reported similar high contribution of coarse NO_3^- to total NO_3^- over India from their EMAC modelling of global aerosols. Studies of ambient measurements in India also conclude that the relatively high fraction of coarse nitrate is related to high levels of dust and/or sea salt over this region (Kumar et al., 2010; Boreddy et al., 2021).

OXS is globally dominated by the SO_4^{2-} aerosol phase (Fig. 2); SO_2 only accounts for more than a few % of OXS in the locality of major SO_2 emissions areas such as eastern China, northern Russia, eastern Kazakhstan, and South Africa. This reflects the fast oxidation of SO_2 to SO_4^{2-} and that OXS mainly exists in the form of SO_4^{2-} during regional transport.

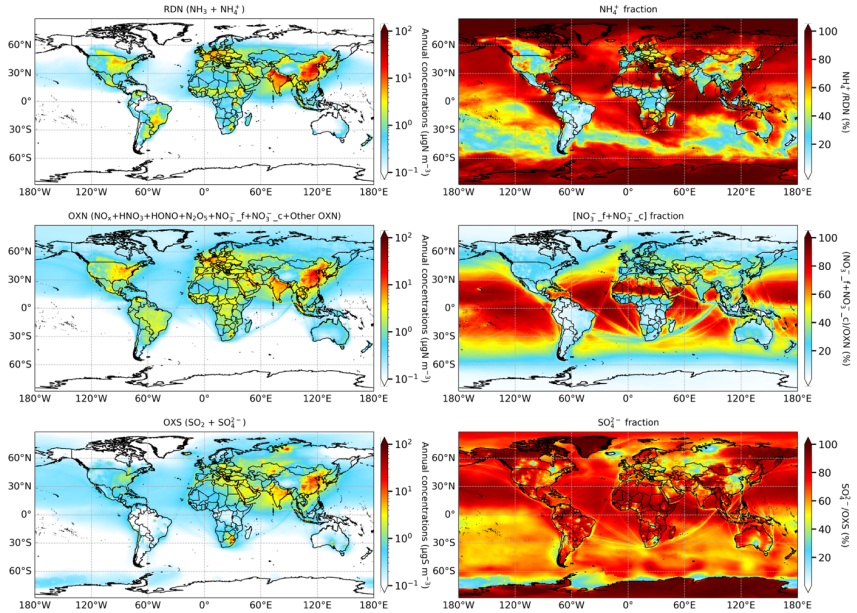

Figure 2: (Left) Annual mean surface concentrations (log scales) and (right) inorganic aerosol-phase fractions of (top) RDN, (middle) OXN, and (bottom) OXS species. The full composition of OXN is listed in Table S1.

3.1.2 Spatial characterisation of SO_4^{2-}-NO_3^--NH_4^+ chemical domains

We apply the concept of chemical domains to characterise the state of ammonia neutralisation of both sulfuric and nitric acids (Metzger et al., 2002b; Metzger et al., 2002a; Hauglustaine et al., 2014; Xu and Penner, 2012; Ansari and Pandis, 1998). Figure 3 shows the global spatial distribution in relative abundances of SO_4^{2-}, fine NO_3^- and NH_4^+ when classified into four such domains. Global maps of the variation in the quantitative species ratios underpinning categorisation into the domains shown in Fig. 3 are presented in Fig. S2a for the ratio of total ammonia T_A to total sulfate T_S, and Fig. S2b for the ratio of free ammonia $T_{A\text{-}free}$ to total nitrate (fine) $T_{N\text{-}f}$. The definitions of these four quantities (in molar concentrations; μmol m^{-3}) are given in equations E1-E4. The SO_4^{2-} in T_S refers to all of H_2SO_4, NH_4HSO_4, $(NH_4)_3H(SO_4)_2$, and $(NH_4)_2SO_4$.

$$T_S = [SO_4^{2-}] \quad (E1)$$

$$T_{N-f} = [HNO_3] + [NO_3^-\_f] \quad (E2)$$

$$T_A = [NH_3] + [NH_4^+] \quad (E3)$$

$$T_{A-free} = T_A - 2 \times T_S \quad (E4)$$

The $T_{A\text{-}free}$ term quantifies the amount of total ammonia that is in excess of that needed to fully neutralise the sulfate, i.e., the T_A remaining when $\frac{T_A}{T_S} > 2$. When $\frac{T_{A-free}}{T_{N-f}} > 1$, sufficient ammonia exits also to fully react with nitrate to from NH_4NO_3. An arbitrary threshold for the sum of the concentrations of fine SO_4^{2-}, NO_3^- and NH_4^+ to be ≥0.5 μg m^{-3} has been applied to Fig. 3 in order to focus attention away from the most remote areas (southern hemisphere oceans and the poles) where fine SIA concentration is very low and knowledge of chemical domain is irrelevant for informing emissions mitigation strategies.

In the blue and yellow areas of Fig. 3, $\frac{T_A}{T_S} < 2$ and sulfuric acid is not fully neutralised and thus not all SO_4^{2-} is in the form of $NH_4(SO_4)_2$. Locations where this ratio is between 1 and 2 are coloured blue in Fig. 3 (green colours in Fig. S2a and grey areas in Fig. S2b) and are defined as 'sulfate-rich.' This is the state over northern hemisphere oceans and remote continental regions such as Sahara Desert, Greenland, and Siberia. Over northern Russia and southern hemisphere oceans, where $\frac{T_A}{T_S} < 1$ (yellow colour in Fig. 3), conditions can be characterised as 'sulfate-very-rich'. As discussed in Sect. 3.1.1, northern Russia is an SO_2 emission hotspot but NH_3 emissions are small. This is also the case around other very large point sources of anthropogenic SO_2 emissions in Kazakhstan, southern Africa and southern Australia. Over ocean areas, biogenic emission of dimethyl sulphide (DMS) is the major source of sulfur in marine aerosol (Fiddes et al., 2018; Jackson et al., 2020) but NH_3 emission is again very small. A separation between sulfate-rich and sulfate-very-rich regions arises because in the former areas there is transport of anthropogenic continental NH_3 emissions over the northern hemisphere oceans. In these sulfate-rich and sulfate-very-rich regions essentially all NH_3 has been converted to NH_4^+ as illustrated in Fig. 2 where RDN concentrations are almost entirely in the form of NH_4^+.

The areas with green and orange colours in Fig. 3 (yellow to red colours in Fig. S2a) have $\frac{T_A}{T_S} > 2$ and consequently $\frac{T_{A-free}}{T_{N-f}} > 0$ (non-grey colours in Fig. S2b) and show where sulfuric acid is fully neutralised and excess NH_3 remains to react with HNO_3 to form NH_4NO_3. Most continental regions with significant SIA pollution are characterised by these conditions including East Asia, Southeast Asia, South Asia, Europe, North America, south-eastern South America, western Africa, and eastern Australia.

The green coloured areas in Fig. 3 have a $\frac{T_{A-free}}{T_{N-f}}$ ratio between 0 and 1 and indicate where NH_3 is the limiting factor for NH_4NO_3 formation and thus where the chemical domain can be characterised as 'NO_3^- rich.' The blue colours in Fig. S2b illustrate the quantitative extent of the HNO_3 neutralisation in these areas. This situation occurs over coastal areas around East Asia, northern Europe, and north-eastern United States. These locations experience transport of oxidised N from the adjacent continent and/or direct shipping emissions of NO_x but NH_3 concentrations are lower because it deposits more quickly to land before transport off the coast.

The orange-coloured areas in Fig. 3 are where $\frac{T_{A-free}}{T_{N-f}} > 1$ and are characterised as 'NH_3 very rich', since here it is the availability of nitrate that limits NH_4NO_3 formation. This condition prevails over most of the temperate and tropical land surface in the northern hemisphere. Concentrations of SIA over a lot of the land in the southern hemisphere are (like over the southern hemisphere oceans) less than the 0.5 μg m^{-3} threshold applied to Fig. 3. Figure S2b shows that the most NH_3-rich areas are in Central Africa, South Asia, East Asia, Southeast Asia, western Europe, South and Central America, North America, and New Zealand where there are intensive agricultural activities and/or large biomass burning and/or low NO_x and SO_x emissions.

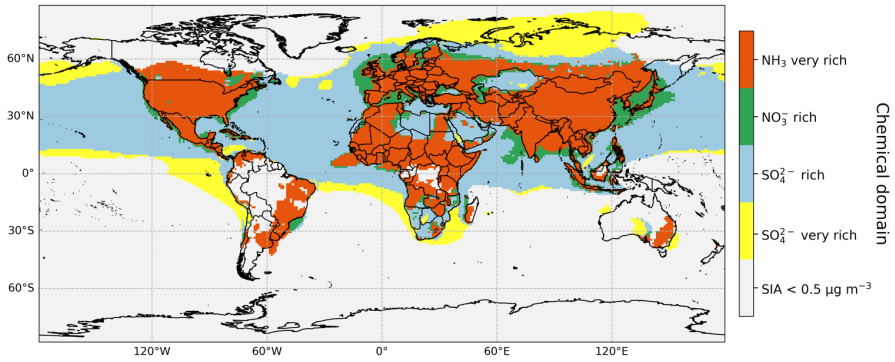

Figure 3: The state of ammonia neutralisation of sulfuric and nitric acids for areas where SIA concentration in the fine particle fraction ($PM_{2.5}$) is ≥0.5 μg m^{-3}. Definitions of the four chemical domains are given in the main text. Maps of the quantitative species ratios underpinning categorisation into these chemical domains are given in Fig. S2.

Hauglustaine et al. (2014) and Xu and Penner (2012) reported similar findings, although both these studies also showed NH_3-very-rich conditions over tropical oceans, which may be related to oceanic NH_3 emissions if these were included in their simulations. They were not included in our model. Oceanic NH_3 emissions are small (~6 TgN yr^{-1}, albeit highly uncertain (Fowler et al., 2015)), compared to continental NH_3 emission (53.1 TgN yr^{-1}; Table 1) and we deliberately exclude discussion of chemical domain where SIA concentration is small.

The continental values of $\frac{T_{A-free}}{T_{N-f}}$ calculated here for 2015 are larger than those reported for 2000. For instance, in western Europe, Xu and Penner (2012) and Hauglustaine et al. (2014) reported $\frac{T_{A-free}}{T_{N-f}}$ ratios of around 1.0-2.0 and 1.0-4.0, respectively, while we report values around 4.0-10.0 (Fig. S2b). This temporal difference is driven not only by the increasing NH_3 emissions associated with sustaining food supply for the growing global population (Sutton et al., 2013; Behera et al., 2013b; Aneja et al., 2009), but also because a growing number of countries have been reducing NO_x and SO_x emissions yet most countries have little or no control policy on NH_3 emissions (Liu et al., 2018; Liu and Matsui, 2021; Aas et al., 2019; de Gouw et al., 2014). These changes in relative emissions of precursors mean an increasingly smaller proportion of gaseous NH_3 is transformed to aerosol NH_4^+, which in turn increases NH_3 concentrations and reduces the effectiveness of $PM_{2.5}$ mitigation via NH_3 emission reductions. For example, Liu et al. (2018) reported a significant growth in gaseous NH_3 concentrations over the North China Plain from 2008 to 2016 allied to the rapid SO_2 emission reductions.

Our results also indicate regional differences in terms of the extent of excess ammonia (Fig. S2b). Table S3 lists the maximum, median and area-weighted mean $\frac{T_{A-free}}{T_{N-f}}$ ratios in different world regions. Among the regions with largest RDN surface concentration, South Asia shows the most 'NH_3-rich' condition with an area-weighted mean ratio of 9.6, followed by South America and Africa whose area-weighted mean ratios are 8.6 and 7.2 respectively. For regions with area-weighted mean $\frac{T_{A-free}}{T_{N-f}}$ ratio > 1, Southeast Asia and Euro_Medi have the lowest area-weighted mean ratios of 1.9 and 2.5, respectively. This lower relative excess of NH_3 of the former is associated with the large proportion of marine area in this region, while the smaller NH_3 abundance in the latter is likely linked to more stringent NH_3 emission targets in Europe than other world regions via the Gothenburg Protocol and EU National Emissions Ceiling Directive.

3.2 Global and regional N_r and S_r deposition

An important advantage of an atmospheric model is that it can apportion the different contributions to deposition that measurements cannot readily quantify. For instance, direct measurements of dry deposition are technically difficult and are very limited in terms of both spatial and temporal coverage. Also, whilst measurement of NH_4^+ in precipitation permits quantification of wet deposition of RDN, it cannot distinguish how much of it derives from rainout of gaseous NH_3 and how much from rainout of particle NH_4^+. Similarly, measurements cannot distinguish between gaseous and particle sources to wet deposition of OXN and OXS. The models therefore provide additional information about the nature of N_r and S_r deposition. This is relevant as the form of deposited N affects the severity of nitrogen deposition impacts (Sutton et al., 2014; Bobbink et al., 2010). An important effect of deposited N gases and aerosols is the direct toxicity to above-ground parts of various plants. Van Herk et al. (2003) found that lichens are particularly sensitive to direct NH_3 dry deposition, whilst Pescott et al. (2015) reported direct toxic effects of wet deposited RDN for bryophytes. Additionally, it must be stressed that the lack of dry deposition comparison between model and measurement, due to the lack of measurement data, means that the numbers reported for modelled dry deposition in this section should be regarded as more uncertain.

Formatted: Font colour: Text 1

3.2.1 RDN

Figure 4 shows the global distribution of annual RDN deposition in 2015 apportioned into dry and wet deposition of each of NH_3 and NH_4^+. The map of total RDN deposition (the sum of all panels of Fig. 4) is provided in Fig. S3. The relative contributions of the different sources of RDN deposition are illustrated in Fig. 5 for the 10 world regions outlined in Fig. 1. The four panels of Fig. 4 show similar spatial patterns of highest depositions over East Asia, South Asia, Europe, eastern North America, south-eastern South America, and central Africa. The greatest RDN deposition (wet + dry) rate occurs in East Asia, exceeding 5300 mgN m^{-2} yr^{-1}. The East Asia region receives more than one-fifth of the world's RDN deposition (Fig. 5). Maximum total RDN deposition in South Asia and Southeast Asia is in the range 3800 to 4600 mgN m^{-2} yr^{-1}, whilst in Europe, North America, South America, and Africa maximum total RDN deposition is in the range 1800 to 2200 mgN m^{-2} yr^{-1} (Fig. S3). These regions each receive 7-11% of global total RDN deposition (Fig. 5). Around 15% of RDN deposition occurs over the oceans ('Rest of World in Fig. 5). In fact, since most of the other world regions also include areas of water, the proportion of global RDN depositing to seas will be greater than 15%.

Globally, the total RDN deposition is 55.5 TgN yr^{-1}, apportioned around 50% each between dry and wet deposition. The global deposition can be further apportioned as 40% NH_3 dry deposition, 9% NH_4^+ dry deposition, 22% wet deposition of NH_3 and 28% wet deposition of NH_4^+ (Table S4). Thus, whilst the large majority (82%) of RDN dry deposition is in the form of NH_3, the RDN wet deposition is more evenly split between rainout of gaseous NH_3 (44%) and rainout of particle NH_4^+ (56%). Overall, 62% and 38% of total global RDN is removed from the atmosphere initially in the form of NH_3 and NH_4^+, respectively.

However, Fig. 5 shows there are large regional variations in the contributions of different sources of RDN deposition. In South Asia, South America, and Oceania more than 50% of RDN deposition is in the form of NH_3 dry deposition. In East Asia, Euro_Medi, North America, and Africa dry deposition of NH_3 is in the range 42-49%. Wet deposition of NH_4^+ is dominant only in remote areas such as Rest of world (54%) and Rest of Asia (40%). Overall, the deposition of NH_3 (dry + wet) accounts for well over half of total RDN deposition in all continental regions (except for Rest of Asia), which indicates that reducing NH_3 emissions will be effective at reducing total RDN input from the atmosphere to continental ecosystems.

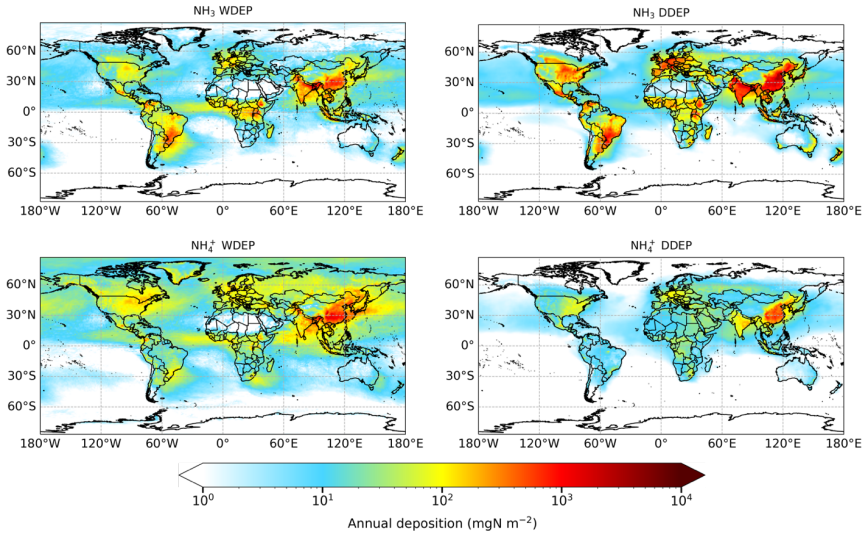

Figure 4: Annual wet (WDEP) and dry deposition (DDEP) of RDN components for 2015. 'NH_3 WDEP' and 'NH_4^+ WDEP' respectively refer to wet deposition of RDN originally present in the atmosphere as gaseous NH_3 or as aerosol NH_4^+. Note the logarithmic scale.

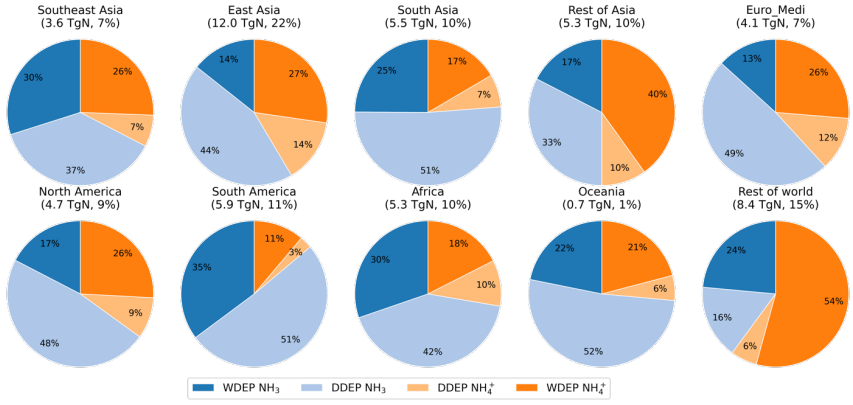

Figure 5: Relative contributions to annual RDN deposition for the set of world regions defined in Fig. 1. The two darker shade colours collectively indicate wet deposition (WDEP), whilst the two lighter shade colours collectively indicate dry deposition (DDEP). The total deposited RDN (TgN) in each region and its proportion to global total RDN deposition are presented below each region name.

3.2.2 OXN

Figure 6 shows the global distribution of annual OXN deposition in 2015 apportioned into dry and wet deposition of gaseous OXN (i.e., NO_x + HNO_3 + HONO + N_2O_5 + other OXN species) and aerosol-phase OXN (NO_3^-_f + NO_3^-_c). The map of total OXN deposition is in Fig. S4. As described above for RDN deposition, model simulations are able to distinguish in detail the ultimate atmospheric source of the OXN deposition, which measurements cannot; in particular to distinguish whether dissolved nitrate in precipitation derives from gas or aerosol-phase species, and which species. The relative contributions of the different sources of OXN deposition for the 10 world regions outlined in Fig. 1 are shown in Fig. 7.

The regions of high OXN deposition in Fig. 6 are similar to those with high RDN deposition (Fig. 4), although shipping NO_x emissions can be seen to have a notable impact on deposition of OXN over a large number of marine locations, which is not apparent for RDN deposition. The largest amounts of total OXN deposition are in East Asia (3300 mgN m^{-2} yr^{-1}), followed by Southeast Asia (2800 mgN m^{-2} yr^{-1}) and South Asia (1700 mgN m^{-2} yr^{-1}) (Fig. S4). However, whilst the East Asia region receives 22% of global RDN deposition (Fig. 5), this region receives only 14% of global OXN deposition (Fig. 7). In North America, maximum OXN deposition is around 1900 mgN m^{-2} yr^{-1}, whilst in Europe it is around 900 mgN m^{-2} yr^{-1}. A greater proportion of OXN deposition occurs over the oceans than is the case for RDN deposition ('Rest of World' proportions are 23% and 15%, respectively), due both to the shipping emissions of NO_x and the longer lifetime (and hence further transport distance) of NO_2 compared with NH_3.

The global total OXN deposition in 2015 is 57.9 TgN yr^{-1}, apportioned as 43% dry deposition and 57% wet deposition. The relative contributions of the individual OXN components to global OXN deposition is shown in Fig. S6. The global deposition is further apportioned as 28% gaseous OXN dry deposition, 15% aerosol-phase OXN dry deposition, 18% wet deposition of gaseous OXN and 39% wet deposition of aerosol-phase OXN (Table S4). The global OXN dry deposition is almost equally split among HNO_3 (34%), coarse NO_3^- (29%), and NO_x (21%, this is effectively dry deposition of NO_2), whereas the rainout of coarse particle NO_3^- (60%) is the predominant form in OXN wet deposition, followed by the rainout of HNO_3 (28%). The dry-deposited fine NO_3^- and the rainout of fine NO_3^- only account for 7% and 9% of OXN dry deposition and OXN wet deposition, respectively. The total deposition (wet + dry) of 'Other' OXN species (predominantly PAN) contributes 5% to global total OXN deposition, and the contributions from HONO and N_2O_5 are negligible. Compared with global RDN deposition, the majority of which derives from wet and dry deposition of gaseous NH_3 (62%), Fig. S6 shows it is coarse particle NO_3^- (46%) that contributes most to global OXN deposition, followed by HNO_3 (30%). Overall, slightly greater OXN deposition derives from aerosol species (54%) than from gaseous species (46%) globally.

Figure 7 shows that the 10 world regions can be viewed in four groups according to the nature of their OXN deposition. A group comprising Southeast Asia, South America and Oceania is characterised by large contributions to total OXN deposition derived from wet and dry deposition of gaseous species. In Southeast Asia, wet and dry deposition of HNO_3 constitutes over half (52%) of total OXN deposition, with coarse NO_3^- (31%) and NO_x (7%) being the second and third contributors. This indicates that it is the formation of gaseous species (mainly HNO_3 and NO_2) that are the most important determinants of OXN deposition in this region. Similar observations are made for South America and Oceania. Fine NO_3^- contributes very little to total OXN deposition in this group of regions.

In the regions of South Asia, Rest of Asia, Africa, and Rest of world, it is coarse NO_3^- (via both wet and dry deposition) that is the most significant contributor to total OXN deposition (wet + dry). This is consistent with the relatively greater abundance of coarse particle NO_3^- in these regions (Fig. S1).

A third group of regions from Fig. 7 comprises North America and Euro_Medi. In these regions, the proportion contributions to total OXN deposition from wet and dry deposition of HNO_3 and coarse NO_3^- are similar at 31-38% and there is also significant contribution from dry deposition of NO_x (13-14%) and 'Other OXN' (6% and 3% for North America and Euro_Medi, respectively). The relative contributions from NO_x in these regions are well above their average contribution globally. There is also an important contribution (8-10%) from wet and dry deposition of fine NO_3^- to total OXN deposition in these two regions.

Finally, the East Asia region is characterised by substantial contribution (24%) to total OXN deposition from wet and dry deposition of fine NO_3^-, a proportion that is more than double the fine NO_3^- contribution in North America and Euro_Medi. The formation of NH_4NO_3 aerosol is therefore an important influence on OXN deposition over East Asia, in addition to its important contribution to $PM_{2.5}$ and to the latter's health effects. The atmospheric components HNO_3 and coarse NO_3^- contribute equal amount (30%) to total wet and dry OXN deposition in East Asia.

Globally, our modelling shows that OXN (51%) and RDN (49%) account for almost equal proportions of the total nitrogen deposition (113.4 TgN yr^{-1}). Other studies report similar values with OXN and RDN deposition amounts each varying in the range 50 to 65 TgN yr^{-1} and contributing comparable amounts to total nitrogen deposition (Hauglustaine et al., 2014; Lamarque et al., 2013; Dentener et al., 2006; Bian et al., 2017; Xu and Penner, 2012; Tan et al., 2018).

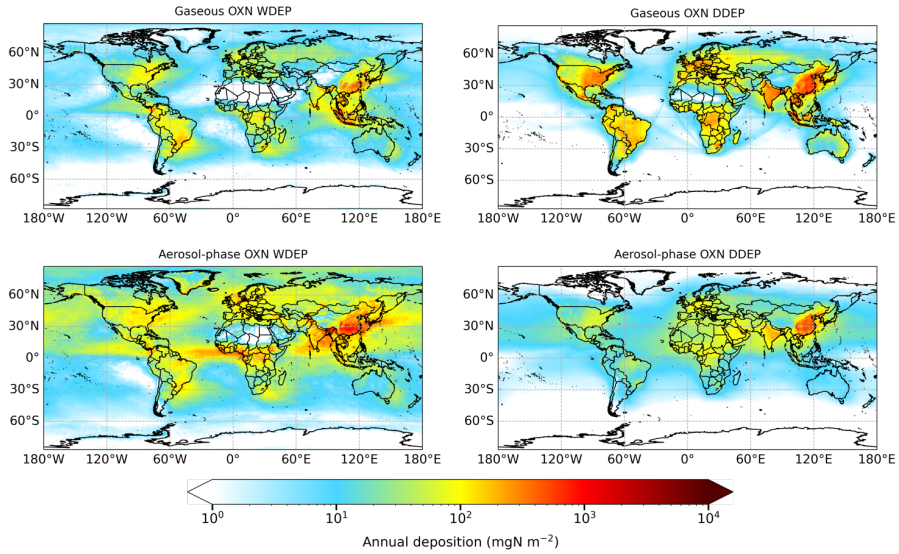

Figure 6: Annual wet (WDEP) and dry deposition (DDEP) of OXN components for 2015. 'Gaseous OXN WDEP' and 'Aerosol-phase OXN WDEP' respectively refer to wet deposition of OXN originally present in the atmosphere as gaseous OXN or as aerosol-phase OXN. The former consists of NO_x, HNO_3, HONO, N_2O_5 and other OXN (predominantly PAN), whilst the latter consists of NO_3^-_f and NO_3^-_c (full compositional details in Table S1). Note the logarithmic scale.

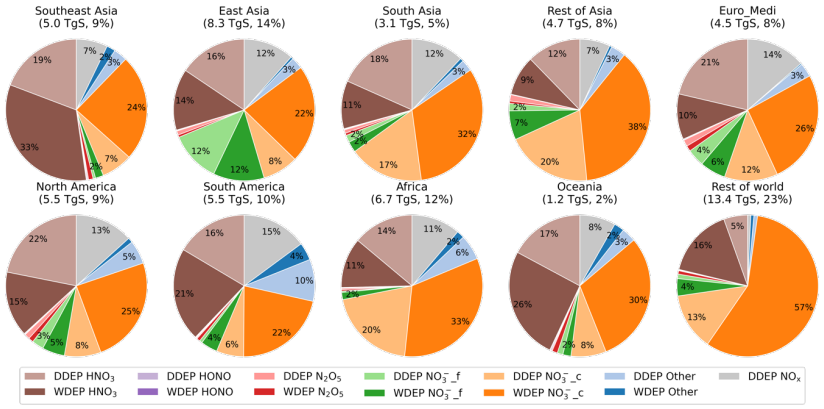

Figure 7: Relative contributions to annual OXN deposition for the set of world regions defined in Fig. 1. Labels for individual contributions <2% are omitted to aid clarity. The darker shade colours collectively indicate wet deposition (WDEP), whilst the lighter shade colours collectively indicate dry deposition (DDEP). The 'Other' OXN species is predominantly PAN (full compositional details in Table S1). The total deposited OXN (TgN) in each region and its proportion to global total OXN deposition are presented below each region name.

3.2.3 OXS

Figure 8 shows the global distribution of annual OXS deposition apportioned into wet and dry deposition of SO_2 and SO_4^{2-}. The map of total OXS deposition is provided in Fig. S5. The relative contributions of the different sources of OXS deposition for the 10 world regions outlined in Fig. 1 are shown in Fig. 9. Higher levels of OXS deposition are found near emission sources in East Asia, South Asia, Europe, eastern United States, and south-eastern Africa for all four deposition components. In addition, both wet and dry deposition of SO_2 is large close to major metal smelting industry such as in northern Russia, where total OXS deposition exceeds 5400 mgS m^{-2} yr^{-1}, eastern Kazakhstan, and South Africa. In East Asia and South Asia, the highest total (wet + dry) OXS depositions are around 4800 mgS m^{-2} yr^{-1} and 2400 mgS m^{-2} yr^{-1}, respectively. OXS deposition in Europe and North America is much smaller, with largest values in the range 900 to 1100 mgS m^{-2} yr^{-1}. A substantial proportion of total OXS deposition occurs over the oceans; 34% occurs over the Rest of world region (Fig. 9), which reflects both deposition of S derived from oxidation of natural DMS emissions, and the longer transport distances of anthropogenic aerosol SO_4^{2-}. Of the continental regions, Fig. 9 shows the greatest proportions of OXS deposition occur in East Asia (16%) and Rest of Asia (11%).

Globally, total OXS deposition in 2015 is 50.5 TgS yr^{-1}, of which 54% is via wet deposition and 46% via dry deposition. The largest contributions to total OXS deposition are wet deposition of aerosol SO_4^{2-} (44%) and dry deposition of SO_2 (35%) (Table S4). Rainout of SO_2 into wet deposition contributes 11% and dry deposition of aerosol SO_4^{2-} contributes 10%. This means that, globally, slightly greater OXS deposition derives from aerosol SO_4^{2-} (54%) than from SO_2 (46%). This is a similar situation to that for OXN deposition but contrasts with RDN deposition for which 62% ultimately derives from the gaseous component (NH_3) and only 38% from the aerosol component (NH_4^+).

The total OXS deposition we calculate for 2015 is around half that reported by Hauglustaine et al. (2014) for 2000 (107 TgS yr^{-1}) and 40% lower than that reported by Tan et al. (2018) for 2010 (84 TgS yr^{-1}). It is also lower than the values for 2000 (range 75-100 TgS yr^{-1}) from a 23 model intercomparison reported by Dentener et al. (2006). The lower OXS deposition value presented here is assumed in part to be due to the considerable reduction in global sulfur emission from 2000 to 2015 (Fowler

et al., 2020; Aas et al., 2019). A direct comparison of modelled S deposition between our work and other studies is confounded by use of different inventories for both anthropogenic and natural emissions.

As for RDN and OXN, the relative contributions of the different sources of OXS deposition vary across the 10 world regions (Fig. 9). However, the regional composition patterns of OXS deposition are broadly similar to those of RDN deposition, with dry deposition of SO_2 (23-46%) and wet deposition of SO_4^{2-} (34-56%) being the two most important contributors in all world regions. Total deposition (wet + dry) of SO_2 and SO_4^{2-} contribute almost equal proportions to total OXS deposition in Southeast Asia, South Asia, North America, South America, and Oceania. In East Asia and Euro_Medi regions, the sum of SO_2 deposition contributes slightly more (55-56%) to total OXS deposition, whereas it is SO_4^{2-} that contributes most (57-67%) to total OXS deposition in Rest of Asia, Africa, and Rest of world.

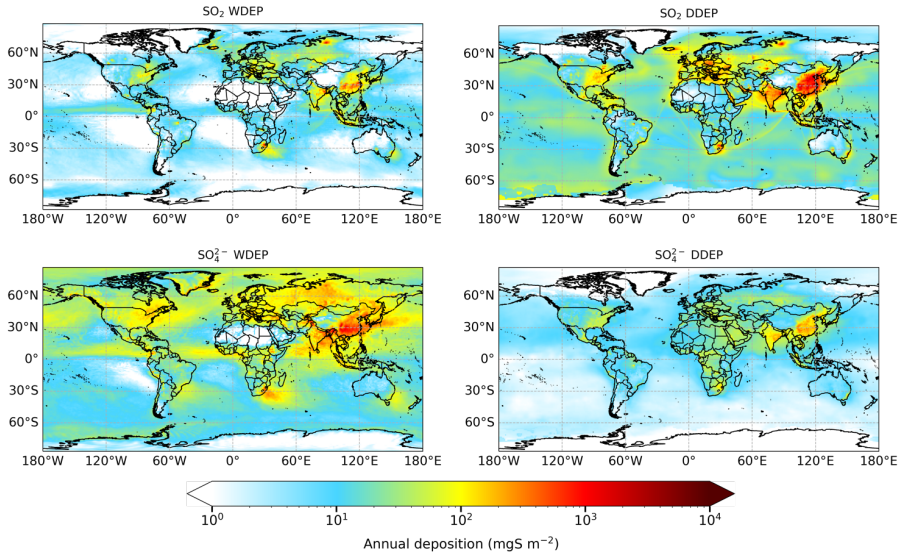

Figure 8: Annual wet (WDEP) and dry deposition (DDEP) of OXS components for 2015. 'SO_2 WDEP' and 'SO_4^{2-} WDEP' respectively refer to wet deposition of OXS originally present in the atmosphere as gaseous SO_2 or as aerosol SO_4^{2-}. Note the logarithmic scale.

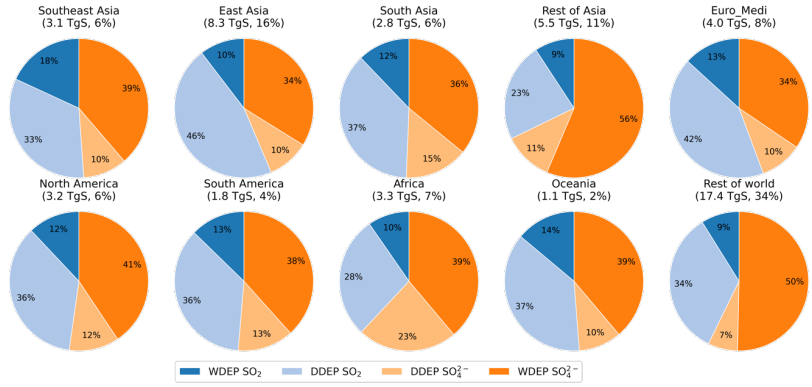

Figure 9: Relative contributions to annual OXS deposition for the set of world regions defined in Fig. 1. The two darker shade colours collectively indicate wet deposition, whilst the two lighter shade colours collectively indicate dry deposition. The total deposited OXS (TgS) in each region and its proportion to global total OXS deposition are presented below each region name.

In summary, on a global basis, wet and dry deposition currently contribute equally to RDN deposition. For OXN and OXS, wet deposition contributes slightly more than dry deposition. These proportions vary regionally according to local precursor emission strengths and climatology. For RDN deposition, dry deposition of NH_3 is the predominant contributor in most regions except for Rest of Asia and Rest of world (essentially oceans) where NH_3 emissions are small and RDN deposition is largely determined by transport of aerosol NH_4^+ from other regions (see Sect. 3.2.1). Further reductions in NH_3 would thus efficiently reduce the deposition of RDN in most world regions. The two largest contributors to OXN deposition in all regions are HNO_3 and coarse NO_3^- (both occurring by both wet and dry deposition). Dry deposition of NO_x (i.e., NO_2) is the third largest contributor in most regions except for East Asia and Rest of world. The deposition of fine NO_3^- is only important over East Asia, and to a lesser extent in Euro_Medi. Due to the general dominance of aerosol-phase NO_3^- in OXN deposition, changes in primary NO_x emissions may not have a direct and linear influence on the deposition of OXN. Sensitivity experiments focusing on the response of deposition to emission changes are required to gain more insight into this issue. For OXS deposition, SO_2 and SO_4^{2-} contribute almost equally to total OXS deposition in most regions. More specifically, the sum of dry deposition of SO_2 and wet deposition of SO_4^{2-} accounts for at least 67% of total OXS deposition in all world regions.

3.3 Global and regional N_r and S_r budgets

3.3.1 Global budgets

Table 1 summarizes global tropospheric budget data for RDN, OXN and OXS for 2015. Table 2 does likewise for the individual components NH_3, NH_4^+, HNO_3, fine NO_3^-, coarse NO_3^-, and SO_4^{2-}. In this study, the top of the troposphere is defined as the top of our model domain at 100 hPa. Table 1 shows that net exchange of chemical species at the top of the model domain ('Flux in' and 'Flux out') is negligible. We calculate atmospheric lifetimes based on both sources and sinks. Detailed calculation procedure is described in Supplement Material Sect. S1.2.

The only source of atmospheric RDN is the annual NH_3 surface emission of 53.1 TgN. The annual average burden of RDN is 0.75 TgN, and it has a global lifetime of 4.9-5.2 days depending on how this is calculated (Table 1). The total deposition of NH_3 is 34.6 TgN yr^{-1} (Table 2). This contributes 62% of the sink of NH_3 and occurs as 65% dry deposition and 35% wet

deposition. Partitioning of NH_3 into NH_4^+ aerosol, which is also the only source of NH_4^+, contributes 21.0 TgN yr^{-1} (38%) to the total sink of NH_3. The NH_4^+ loss comes mainly from wet deposition, 15.8 TgN yr^{-1} (76%), and to a lesser extent from dry deposition, 5.02 TgN yr^{-1} (24%). Net loss to the stratosphere is negligible. The global average tropospheric lifetime of NH_4^+ (8.9 days) is much longer than that of NH_3 (1.6 days), consistent with the annual average NH_4^+ burden (0.51 TgN) being more than double that of NH_3 (0.24 TgN) (Table 2).

Xu and Penner (2012), Hauglustaine et al. (2014) and Bian et al. (2017) report similar global total NH_3 emissions (50.5-53.6 TgN yr^{-1} for 2000, and 51.8 TgN yr^{-1} for 2008), but smaller burdens and shorter lifetimes of NH_3 and NH_4^+ than we report here. The burdens of NH_3 and NH_4^+ are 0.07 TgN (lifetime = 0.46 days) and 0.26 TgN (lifetime = 3.23 days) in Xu and Penner (2012), and 0.09 TgN (lifetime = 0.63 days) and 0.22 TgN (lifetime = 4.52 days) in Hauglustaine et al. (2014) for 2000. Burdens of NH_3 and NH_4^+ averaged across 9 models in Bian et al. (2017) for 2008 are 0.16 TgN and 0.25 TgN with a corresponding lifetime of 0.72 days and 4.3 days. It is important to note that the NH_3 burden across the 9 models in Bian et al. (2017) varied by a factor of 17. This indicates the sensitivity of burdens and lifetimes of NH_3 and NH_4^+ to the definition of model domain, the deposition pathways, and the interactions between NH_3 and acidic species in different models.

Table 1: Global tropospheric budgets of total RDN, OXN, and OXS in 2015. Flux (out - in) = Flux out - Flux in. *Q* is the annual average burden, *P* is the production pathway (i.e., sources), *R* is the removal pathway (i.e., sinks), and τ is atmospheric lifetime. The constituents of the three groups are listed in Table S1.

	Total RDN	Total OXN	Total OXS
Sources (TgN/TgS yr^{-1})	53.1	56.6	48.5
Sinks (TgN/TgS yr^{-1})	55.5	57.9	50.5
Dry deposition	27.4	24.7	23.1
Wet deposition	28.1	33.2	27.4
Chemical loss	-	-	-
Flux (out - in)	0.01	0.01	-0.04
Burden (TgN/TgS)	0.75	1.20	0.78
Lifetime (days): $\tau = \frac{Burden}{Sources}$	$\frac{Q(NH_3 + NH_4^+)}{P(NH_3)}$	$\frac{Q(OXN)}{P(NO_X)}$	$\frac{Q(SO_2 + SO_4^{2-})}{P(SO_2)}$
	5.2	7.7	5.9
Lifetime (days): $\tau = \frac{Burden}{Sinks}$	$\frac{Q(NH_3 + NH_4^+)}{R(NH_3 + NH_4^+)}$	$\frac{Q(OXN)}{R(OXN)}$	$\frac{Q(SO_2 + SO_4^{2-})}{R(SO_2 + SO_4^{2-})}$
	4.9	7.6	5.6

The global atmospheric OXN source and sink flux is 56.6 and 57.9 TgN yr^{-1} (Table 1). The annual average OXN burden is 1.20 TgN, with a global mean lifetime of 7.6 or 7.7 days depending on how this is calculated. Detailed global budgets of HNO_3 and fine and coarse NO_3^- are listed in Table 2. As quantification of the flux of HNO_3 through photolysis and reaction with OH is not available as model output, the HNO_3 budget presented here includes only deposition and aerosol nitrate formation. Xu and Penner (2012) and Hauglustaine et al. (2014) report that 6.9%-10% of HNO_3 loss occurs via photolysis and reaction with OH, so these loss routes are relatively small. The total chemical production of HNO_3 in our study is 49.5 TgN

yr^{-1}, which is 17% higher than the 42.3 TgN yr^{-1} reported by Xu and Penner (2012), and 2% higher than the 48.5 TgN yr^{-1} in Hauglustaine et al. (2014). The total loss of HNO_3 is 49.4 TgN yr^{-1}, of which 17.6 TgN yr^{-1} (36%) is removed from the atmosphere by deposition, almost equally via dry deposition (8.35 TgN yr^{-1}) and via wet deposition (9.25 TgN yr^{-1}). The remaining 64% of the HNO_3 loss goes into formation of 4.54 TgN yr^{-1} fine nitrate (14% of the aerosol nitrate source) and 27.2 TgN yr^{-1} coarse nitrate (86% of the aerosol nitrate source). The tropospheric annual average burden of HNO_3 is 0.15 TgN with a lifetime of 1.1 days.

The loss of fine and coarse nitrate is only via deposition, and 72% of total nitrate loss is due to wet deposition. The calculated nitrate lifetimes range between 4.8 and 7.1 days, which are in line with lifetimes (4.6-6.3 days) reported in other studies (Xu and Penner, 2012; Hauglustaine et al., 2014; Bian et al., 2017). Coarse nitrate (7.0-7.1 days) has slightly longer lifetime than fine nitrate (4.8 days). Our calculated total nitrate annual average burden is 0.58 TgN with fine NO_3^- comprising only 10% of this total. This total nitrate burden is around three times greater than the value in Xu and Penner (2012) and Hauglustaine et al. (2014) for 2000 (0.17-0.18 TgN), which likely reflects a shift in gas-aerosol partitioning between 2000 and 2015 from gas-phase HNO_3 more towards aerosol-phase NO_3^-, especially given that their HNO_3 burden of 0.30 TgN is double our value. It is also possible that the simulation of nitrate burdens is more sensitive to coarse particle emissions and the production of coarse nitrate in our model than in models used by Xu and Penner (2012) and Hauglustaine et al. (2014).

The dominance of coarse nitrate in global total nitrate burden is also observed in other global modelling studies. Hauglustaine et al. (2014), Xu and Penner (2012), and Bauer et al. (2007) reported a relative contribution of coarse-mode nitrate of 72%, 77%, and 79% to total nitrate burden in their respective models for 2000. Additionally, the lifetime of fine nitrate calculated in our work is comparable with other literature values. Park et al. (2004) reported a global fine nitrate lifetime against deposition of 3.2 days for 2001, Feng et al. (2007) reported a global lifetime of total nitrate (fine + coarse) of 5.0 days for 1997, and Alexander et al. (2020) reported a global lifetime of inorganic nitrate (HNO_3 + total NO_3^-) for the period 2000-2015 on the order of 3–4 days.

For OXS, emission of SO_2 is the only source, and deposition (wet + dry) is almost the only sink pathway (Table 1). The annual average burden of OXS is 0.78 TgS with a lifetime of 5.6-5.9 days depending on how it is calculated. The total source of SO_4^{2-} is 27.6 TgS yr^{-1} (Table 2). The dominant loss of SO_4^{2-} is wet deposition (81%) with the remaining loss (19%) being dry deposition. The annual average SO_4^{2-} burden in the troposphere is 0.63 TgS. SO_4^{2-} lifetime of 8.3-8.5 days is very similar to the NH_4^+ lifetime, which can be explained by the close chemical association between these two species in atmospheric SIA.

Table 2: Global tropospheric budgets of NH_3, NH_4^+, HNO_3, NO_3^- and SO_4^{2-} in 2015. Flux (out - in) = Flux out - Flux in. *Q* is the quantity of annual average burden, *P* is the production pathway (i.e., sources), *R* is the removal pathway (i.e., sinks), and τ is atmospheric lifetime.

	NH_3	NH_4^+	HNO_3	NO_3^-_f	NO_3^-_c	SO_4^{2-}
Sources (TgN/TgS yr^{-1})	53.1	21.0	49.5	4.54	27.2	27.6
Sinks (TgN/TgS yr^{-1})	55.6	20.8	49.4	4.52	26.9	27.2
Dry deposition	22.4	5.02	8.35	1.66	7.05	5.24
Wet deposition	12.2	15.8	9.25	2.87	19.8	22.0
Chemical loss	21.0	-	31.8	-	-	-
Flux (out - in)	0.00	0.01	0.00	-0.01	0.02	0.00
Burden (TgN/TgS)	0.24	0.51	0.15	0.06	0.52	0.63

	$\frac{Q(NH_3)}{P(NH_3)}$	$\frac{Q(NH_4^+)}{P(NH_4^+)}$	$\frac{Q(HNO_3)}{P(HNO_3)}$	$\frac{Q(NO_3^-\_f)}{P(NO_3^-\_f)}$	$\frac{Q(NO_3^-\_c)}{P(NO_3^-\_c)}$	$\frac{Q(SO_4^{2-})}{P(SO_4^{2-})}$
Lifetime (days): $\tau = \frac{Burden}{Sources}$	1.6	8.9	1.1	4.8	7.0	8.3
Lifetime (days): $\tau = \frac{Burden}{Sinks}$	$\frac{Q(NH_3)}{R(NH_3)}$	$\frac{Q(NH_4^+)}{R(NH_4^+)}$	$\frac{Q(HNO_3)}{R(HNO_3)}$	$\frac{Q(NO_3^-\_f)}{R(NO_3^-\_f)}$	$\frac{Q(NO_3^-\_c)}{R(NO_3^-\_c)}$	$\frac{Q(SO_4^{2-})}{R(SO_4^{2-})}$
	1.6	8.9	1.1	4.8	7.1	8.5

Differences in species lifetimes underpin the differences in vertical and horizontal distributions of the species. For example, as discussed in Sect. 3.1.1, gaseous NH_3, with a short lifetime, only shows dominant contribution to total RDN surface concentration in places near emission sources, whereas aerosol-phase NH_4^+, as a RDN reservoir species with a longer lifetime, is the major form of RDN over the remote continental regions and oceans.

The vertical distributions of N_r and S_r species shown in Fig. 10 also reflect the different species lifetimes. All species exhibit strong vertical gradients of decreasing concentration from the surface up to 10 km. The gaseous species (NH_3, NO_2 and SO_2) have peak concentrations at the surface between 20-40°N as shown in their surface distribution maps (Sect. 3.1.1). These gaseous species are emitted at the surface and their lifetimes are too short for significant mixing to high altitudes. Between the model surface layer (~50 m) and ~2.5 km the maximum zonal mean of NH_3 and SO_2 decreases from 1.77 μg m^{-3} to 0.31 μg m^{-3}, and from 1.78 μg m^{-3} to 0.23 μg m^{-3}, respectively, whereas the concentration gradient of NO_2 is steeper, with maximum zonal mean decreasing from 4.11 μg m^{-3} to 0.10 μg m^{-3}, reflecting that production and removal processes of NO_2 mainly occur in the surface layer.

In contrast, the secondary species NH_4^+, NO_3^- (fine + coarse) and SO_4^{2-} are mixed to higher altitudes than their precursors. The zonal mean concentrations of the secondary species also show a larger horizontal variation range (10-60°N), again reflecting their longer transport times. A notable observation from Fig. 10 is that the maximum concentrations of the secondary aerosol species are not at the surface, a feature that will not be apparent from surface measurements of these species. The maximum zonal mean of NH_4^+ (1.20 μg m^{-3}) and SO_4^{2-} (2.58 μg m^{-3}) occurs in the model level 88-177 m above the surface, whilst maximum NO_3^- (3.80 μg m^{-3}) occurs in the 177-313 m model level. These elevated maxima in secondary components reflect their lack of surface emission and the time taken for the in-atmosphere oxidation and gas-to-particle chemistry.

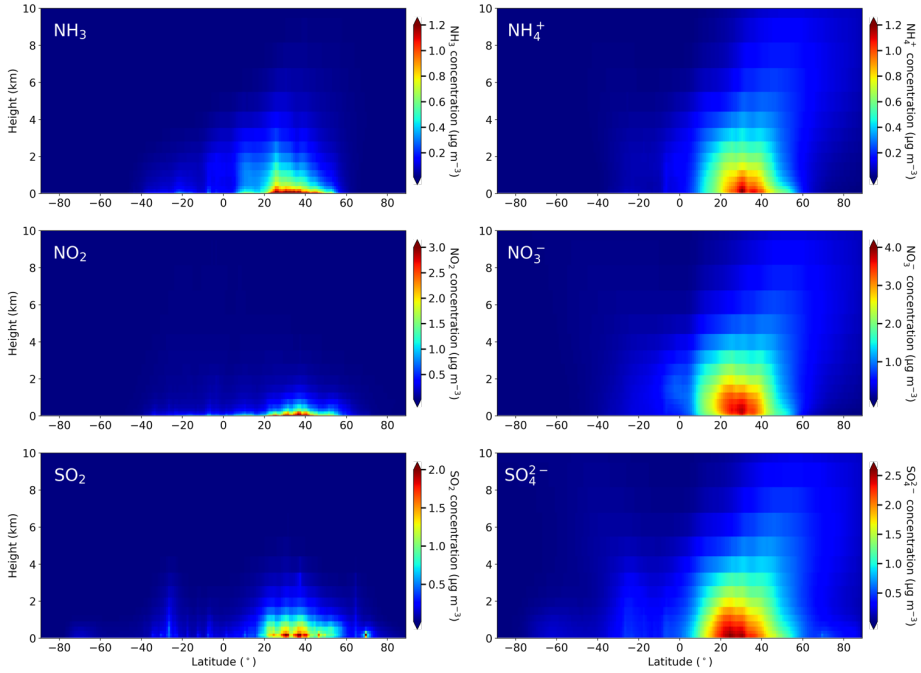

Figure 10: Annual zonal mean vertical concentrations of NH_3, NH_4^+, NO_2, NO_3^- (fine + coarse), SO_2 and SO_4^{2-}.

3.3.3 Regional budgets

Figure 11 shows the differences between annual emissions and depositions for RDN, OXN, and OXS in the 10 world regions illustrated in Fig. 1. The corresponding absolute emission and deposition fluxes for each region are presented in Fig. S7.

For continental regions, the maximum fluxes for RDN are in East Asia (12.5 TgN yr^{-1} for RDN emission and 12.0 TgN yr^{-1} for RDN deposition), followed by South Asia (7.67 TgN yr^{-1} emission and 5.46 TgN yr^{-1} deposition) (Fig. S7). Both these regions are characterised by intensive agricultural activities and have RDN fluxes that are larger than the OXN fluxes. Fluxes of RDN in North America, Euro_Medi and Southeast Asia regions are lower (3.46-5.14 TgN yr^{-1}). The spatial distribution of RDN concentrations presented in Fig. 2 are the consequence of these regional variations in RDN fluxes. Figure 11 shows that all regions are net exporters of RDN except for Southeast Asia and Rest of world in which marine areas dominate. The net import of RDN in Southeast Asis is, however, very small. In contrast, deposition of RDN in the Rest of world region is nearly 16 times its annual emissions. The difference of 7.89 TgN yr^{-1} shows that RDN deposition is a notable source of continental anthropogenic pollution to the oceans. The region with greatest export of RDN is South Asia, at 2.21 TgN yr^{-1} or 29% of its annual emissions (Fig. 11). Euro_Medi and Africa have the next greatest net exports, of 1.08 TgN yr^{-1} (21% of emissions) and 0.95 TgN yr^{-1} (15% of emissions), respectively. The relative differences between emissions and depositions over North America, South America and Oceania are in the range 6.0- 8.0%. Although East Asia is the region with greatest RDN emissions, it only exports 3.8% (0.48 TgN yr^{-1}). This region is geographically generally self-contained from the other regions

but means that East Asia is largely responsible for its own RDN pollution. The relatively high availability of acidic species also leads to shorter chemical lifetimes in this region.

For OXN, East Asia and Africa are the two continental regions with the largest annual emission and deposition fluxes (6.72-9.59 TgN yr^{-1}), followed by South America and North America (5.49-7.02 TgN yr^{-1}) (Fig. S7). In all of Southeast Asia, Euro_Medi, North America, South America, Africa, Oceania, and Rest of world the OXN fluxes have larger influence on their total nitrogen budgets than the RDN fluxes, whereas, as noted above, in East Asia and South Asia fluxes of RDN comprise the majority. In contrast to our finding of higher RDN flux in East Asia (12.0-12.5 TgN yr^{-1}) than OXN flux (8.33-9.59 TgN yr^{-1}), Tan et al. (2018) report higher OXN fluxes (10.5-11.4 TgN yr^{-1}) than RDN fluxes (7.7-8.5 TgN yr^{-1}). Such difference in RDN and OXN fluxes is partially attributed to differences in emission inventories, model structures, meteorology input, and region definition between the two studies. It may also reflect an increase in NH_3 emissions and a reduction in NO_x emissions in this region between 2015 and 2010.

Figure 11 shows that the continental region with the greatest net export of OXN (1.92 TgN yr^{-1}, 22% of emissions) is Africa, followed by Euro_Medi (1.61 TgN yr^{-1}, 26%), South Asia (1.57 TgN yr^{-1}, 34%), and South America (1.51 TgN yr^{-1}, 22%). In particular, OXN deposition over Rest of world (13.4 TgN yr^{-1}) is around 5 times larger than its emission (2.21 TgN yr^{-1}, from shipping). The difference of 11.2 TgN yr^{-1} between OXN deposition and emission in this region is greater than the 7.89 TgN yr^{-1} difference for RDN. It is likely that the oxidation of NO_x to reservoir organic nitrate species such as PAN facilitates the long-distance transport of OXN from the continent to the ocean, whereas the short lifetime of NH_3 means less RDN is transported from its continental emissions regions. Regardless of the explanation, the very large net deposition of OXN in the Rest of world region again indicates the scale of anthropogenic N deposition to marine areas.

Considering OXS, Fig. S7 shows that the Rest of world region has both the largest emission (10.6 TgS yr^{-1}) and deposition (17.4 TgS yr^{-1}) fluxes. The former is due to the substantial marine DMS emissions whose atmospheric oxidation ultimately produces SO_2 and H_2SO_4 (Marandino et al., 2013; Schobesberger et al., 2013; Hoffmann et al., 2016). These OXS emissions largely deposit back to the oceans, but Fig. 11 shows that OXS deposition in the Rest of world is also substantially augmented by long-range transport of OXS pollution from other regions. For continental regions, East Asia has the largest OXS fluxes, with emission and deposition reaching 8.95 TgS yr^{-1} and 8.30 TgS yr^{-1}, respectively, followed by Rest of Asia (5.48-6.21 TgS yr^{-1}) and Euro_Medi (4.05-5.57 TgS yr^{-1}) (Fig. S7). South Asia is the largest net exporter of OXS with 1.62 TgS yr^{-1} (37% of its emission) being deposited outside this region (Fig. 11). Euro_Medi is the second largest net exporter of OXS (1.52 TgS yr^{-1}, 27%). All other continental regions are also either positive or negligible exporters of OXS except for Southeast Asia which receives more OXS depostion than it emits. This is similar to the situation for RDN because away from major NO_x emission areas NH_4^+ is predominantly associated with SO_4^{2-}.

Deleted: This likely reflects

Deleted: reductions

Deleted: (our results)

Deleted: (Tan et al., 2018).

Deleted: desposition

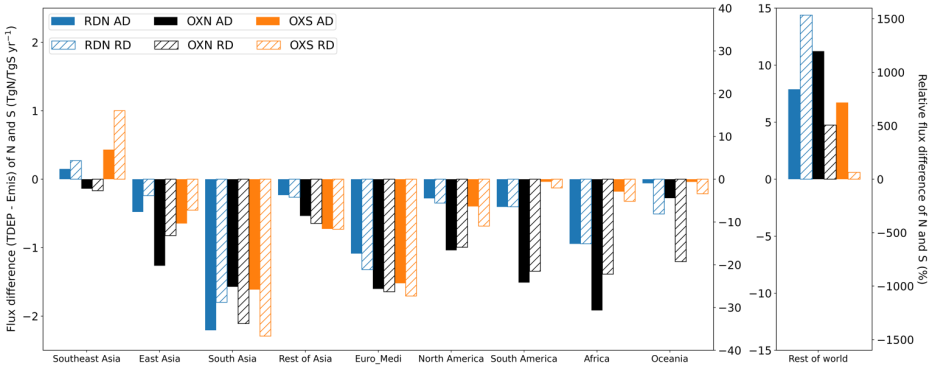

Figure 11: Absolute (AD) and relative differences (RD) between emission and deposition fluxes of RDN (TgN yr^{-1}), OXN (TgN yr^{-1}), and OXS (TgS yr^{-1}) for the 10 world regions defined in Fig. 1. Relative differences are expressed relative to emission fluxes. Difference values for the 'Rest of world' region are much larger than for other regions. The constituents of RDN, OXN and OXS are listed in Table S1. The corresponding emission and deposition fluxes are shown in Fig. S7.

The tropospheric burden of each species is around one or two orders of magnitude smaller than its corresponding emission/deposition flux. Figure 12 and Fig. S8 respectively show, for each of the 10 world regions, the relative and absolute contributions of individual RDN and OXN species to the total tropospheric N burden, and the contributions of the individual OXS species to the total tropospheric S burden. In Table 3, we present the regional atmospheric lifetimes of RDN, OXN and OXS as quantified against their total emission or deposition fluxes. These regional lifetimes are not fully accurate because they do not take into account the net transport of RDN, OXN or OXS across the boundary of the region. However, given that, aside from the Rest of world region, the net transport in/out of a region is relatively small compared to the emission and deposition fluxes (Fig. 11), they should be reasonable estimates of the regional RDN, OXN and OXS lifetimes. Table 3 shows that the regional RDN, OXN and OXS lifetimes vary by up to a factor of 4 across the continental regions, being generally longest over Africa and Rest of Asia, where population and emissions are generally less dense, and shortest over East Asia, Southeast Asia and South Asia.

Deleted: S5

Deleted: S5

The Rest of world region has the highest burdens of all regions with 0.23 TgN RDN, 0.44 TgN OXN, and 0.27 TgS OXS, representing 31%, 37%, and 35% of global RDN, OXN and OXS burdens respectively, despite the relatively small emissions for RDN and OXN from this region. This observation is consistent with the conclusions from analyses of regional emission/deposition fluxes in Fig. 11 that the ocean areas are substantially impacted by transport of N_r and S_r air pollutants from continental regions. The lifetimes of RDN, OXN, and OXS in Rest of world are also the longest of all regions (Table 3), reflecting that RDN, OXN, and OXS in this region predominantly exist as longer-lived species: SO_4^{2-} in the case of S_r, and NH_4^+, NO_3^- and 'Rest OXN' (predominantly PAN) in the case of N_r. East Asia, Rest of Asia, and Africa have moderate burdens of 0.09-0.11 TgN (12%-14% of global burden) for RDN, 0.10-0.16 TgN (9%-13%) for OXN, and 0.08-0.12 TgS (11%-16%) for OXS. South Asia, Euro_Medi, and North America have smaller burdens with their contributions to global burdens ranging from 6%-9% for RDN, 4%-7% for OXN, and 5%-8% for OXS.

Deleted: S5

The species contributions to N burdens differ between the regions (Fig. 12). RDN contributes 58% and 49% to total N burden in South Asia and East Asia, respectively, which is similarly reflected in the emission and deposition fluxes in the two regions, followed by Rest of Asia (42%) and Euro_Medi (39%). The largest relative contributions of OXN to total N burden are in Oceania (82%) and South America (70%).

The largest contribution of NH_3 to RDN burden is in South America (67%) and this large proportion of NH_3 gives South America the shortest RDN lifetime (1.8-1.9 days) of any region. In other parts of the world, NH_4^+ is the majority contributor to RDN burden. The RDN lifetime in Southeast Asia and East Asia is relatively short (2.6-3.0 days), while Rest of Asia has the longest RDN lifetime (7.0-7.3 days) except for Rest of World.

For OXN, the contribution of HNO_3 to the OXN burden reaches 28%, 24% and 22% in Southeast Asia, Oceania, and South America, respectively, whereas HNO_3 contributes only 5%-12% to OXN in other parts of the world (Fig. 12). NO_3^-_f only makes a significant contribution (20%) to total OXN burden over East Asia; its contribution is <6% in other regions. This reflects the strong propensity for NH_4NO_3 formation in East Asia, which is similarly shown in the composition pattern of OXN deposition in this region as well (Sect. 3.2.2). Coarse NO_3^- is a significant contributor to OXN burden, particularly in South Asia (59%), Rest of Asia (54%), and Africa (52%). This is associated with an abundance of coarse particles like sea salt, dust, and sand in these regions. It is therefore critical to correctly account for contributions of coarse nitrate in models as it overwhelmingly controls atmospheric nitrate burden and determines the size distribution of nitrate aerosol. In all world regions SO_4^{2-} is the predominant form of the OXS burden (Fig. 12).

To mitigate atmospheric N_r and S_r burdens and their associated impacts on human health and ecosystems, tackling secondary inorganic species like NH_4^+, and coarse NO_3- and their precursors should be prioritised. The impacts of possible emission controls on atmospheric N_r and S_r concentrations, depositions, budgets, and lifetimes can be quantified by the emission sensitivity tests. Results from these experiments will be discussed in separate publication.

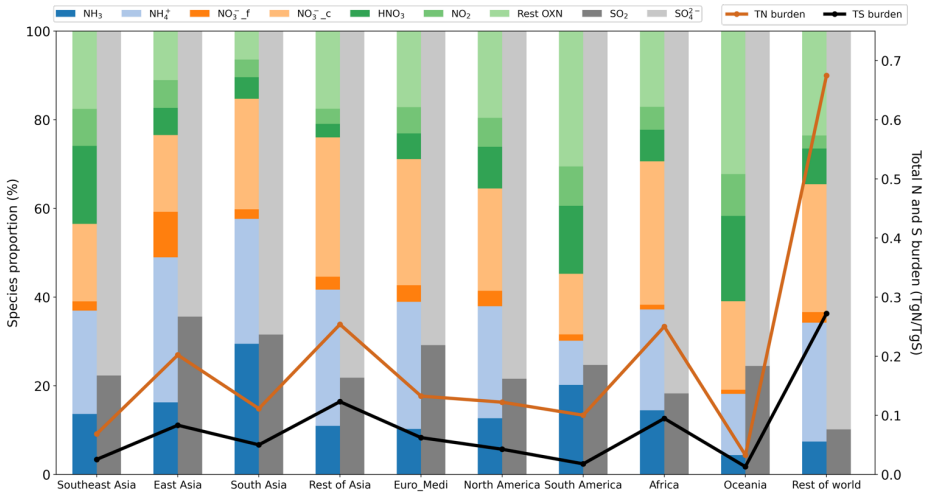

Figure 12: Relative compositions of the tropospheric burdens in 2015 (stacked bar plots, left *y* axis) of total N (RDN + OXN) and total S (OXS) for the 10 world regions defined in Fig. 1. The total N (RDN + OXN) and S regional burdens are shown as the line plots (right y axis). 'Rest OXN' includes HONO, N_2O_5 and other OXN species (full listing given in Table S1).

Formatted: Font colour: Auto

Table 3: Regional atmospheric lifetimes for RDN, OXN and OXS calculated using either total emission or deposition fluxes. *Q* is the burden, *P* is the production pathway (i.e., emissions), *R* is the removal pathway (i.e., depositions), and τ is atmospheric lifetime. These regional lifetimes are not fully accurate because they do not take into account the net transport of RDN, OXN or OXS across the boundary of the region, but these are relatively small for most continental regions. Please note that the lifetimes derived from the production pathway for Rest of world are not listed in this table because these numbers are highly skewed by the the net transport of RDN, OXN and OXS from other regions (full data is available in Table S5).

(days)	Southeast Asia	East Asia	South Asia	Rest of Asia	Euro_Medi	North America	South America	Africa	Oceania	Rest of world
					RDN					
$\tau = \frac{Q}{P}$	2.7	2.9	3.1	7.0	3.7	3.4	1.8	5.4	2.9	-
$\tau = \frac{Q}{R}$	2.6	3.0	4.3	7.3	4.6	3.6	1.9	6.4	3.2	10
					OXN					
$\tau = \frac{Q}{P}$	3.1	3.9	3.7	10	4.8	4.2	3.6	6.6	6.8	-
$\tau = \frac{Q}{R}$	3.1	4.5	5.6	12	6.6	5.0	4.6	8.5	8.4	12
					OXS					
$\tau = \frac{Q}{P}$	3.4	3.4	4.2	7.2	4.1	4.3	3.6	9.9	4.2	-
$\tau = \frac{Q}{R}$	3.0	3.7	6.6	8.2	5.6	4.8	3.7	10	4.4	5.7

The model evaluation presented in Ge et al. (2021) shows that the model-measurement bias varies from one pollutant to another. For instance, the model underestimates annual global HNO_3 surface concentration measurement by 34%, but overestimates NO_2 by 23%. Although it is difficult to diagnose the extent to which bias is contributed by bias intrinsic to the model, including in emissions input to the model, or to bias in measurements, or to measurement-model spatial representation mismatch, it is important to acknowledge that all numbers reported in this work may be biased somewhat low/high.

The intention here is to provide a new overview of how N_r and S_r budgets vary among different world regions and among different chemical species. Since Ge et al. (2021) show that the EMEP model is capable of capturing the overall spatial variation of surface concentrations for major N_r and S_r pollutants and their wet deposition, and since our results are comparable with similar global modelling studies, we have confidence that we characterise the major regional differences in budgets. However, we also acknowledge that there are varying uncertainties in different regions, as revealed by our model evaluation study (Ge et al., 2021). We therefore have greater confidence in regional budgets in North America, Europe, and Southeast Asia than other world regions. But whether different regional uncertainties derive from the emissions, model processes, measurements, or a combination of these aspects, is impossible to resolve only from a modelling study. Further evaluation studies of emissions and measurements are required to grain more insight.

4 Conclusions

We used the EMEP MSC-W model 4.34 coupled with WRF 4.2.2 meteorology to undertake a new present-day evaluation of global and regional concentrations, wet and dry deposition, fluxes and lifetimes of reactive N and S species. These are quantities that cannot be derived from measurements alone. Simulations used the 2015 ECLIPSE annual emissions with EDGAR monthly profiles. Surface concentration and wet deposition outputs from this model configuration have been comprehensively evaluated against several measurement networks.

Our simulations show that the largest surface concentrations and deposition of RDN (NH_3 + NH_4^+), OXN (NO_x + HNO_3 + HONO + N_2O_5 + NO_3^-_f + NO_3^-_c + other OXN species), and OXS (SO_2 + SO_4^{2-}) are in eastern China and northern India. In these areas RDN concentrations are predominantly in the form of NH_3 (NH_4^+ is typically <20%), as also in Europe and North America. NH_4^+ comprises >90% of RDN over oceans and remote continental areas. Gaseous OXN species constitute the majority of OXN over continental regions, whereas NO_3^- dominates OXN over oceans, except for major shipping routes. In eastern China, Europe, and eastern North America fine NO_3^- dominates nitrate, but in India coarse NO_3^- dominates, as has

Deleted: The

been noted elsewhere. Aerosol SO_4^{2-} is the major form of OXS nearly everywhere except in the vicinity of very large SO_2 emission sources.

Most continental regions are now characterised as 'ammonia rich', which indicates that whilst reducing NH_3 emissions will decrease RDN concentration and deposition it will have little effect on mitigating secondary inorganic aerosol. Our results show an increase in ammonia richness compared with model simulations for 2000 in other studies. This is driven not only by increasing NH_3 emission in parts of the world, but also because a growing number of countries have been reducing NO_x and SO_x emissions much faster than NH_3, for which many countries have yet to set emissions targets. In general, South Asia shows the most ammonia-rich condition. Coastal areas around East Asia, northern Europe, and north-eastern United States can be characterised as 'nitrate rich' where NH_4NO_3 formation is limited by NH_3 not nitrate. These locations experience transport of oxidised N from the adjacent continent and/or direct shipping emissions of NO_x but NH_3 concentrations are lower because it deposits more quickly to land before transport off the coast.

Our modelling shows that OXN (57.9 TgN yr^{-1}, 51%) and RDN (55.5 TgN yr^{-1}, 49%) account for almost equal proportions of the total nitrogen deposition. Total sulphur (OXS) deposition is 50.5 TgS yr^{-1}. Globally, wet and dry deposition contribute equally to RDN deposition. For OXN and OXS, wet deposition contributes slightly more than dry deposition. However, the contributions of different deposition components vary regionally. An advantage of modelling is that it can distinguish the individual deposition processes, which measurements cannot. For example, the model shows that in many regions the majority of the wet deposition of RDN derives from rainout of gaseous NH_3 rather than of particle NH_4^+. For RDN deposition, dry deposition of NH_3 is the predominant contributor in most regions except for Rest of Asia and Rest of world (essentially oceans) where NH_3 emissions are small and RDN deposition is largely determined by transport of aerosol NH_4^+ from other regions. Further reductions in NH_3 would thus efficiently reduce the deposition of RDN in most world regions. The two largest contributors to OXN deposition in all regions are HNO_3 and coarse NO_3^- (both occurring by both wet and dry deposition). The deposition of fine NO_3^- is only important over East Asia (24%) and is <10% in other regions. For OXS deposition, dry deposited SO_2 and wet deposited SO_4^{2-} are two largest contributors in all regions.

The annual average tropospheric burden of RDN is 0.75 TgN of which NH_3 and NH_4^+ comprise 32% (0.24 TgN) and 68% (0.51 TgN) respectively. The average tropospheric lifetime of NH_3 is 1.6 days, while that of NH_4^+ is more than 5 times longer (8.9 days). The annual average burden of HNO_3 is 0.15 TgN with an average lifetime of only 1.1 days. Total nitrate burden is 0.58 TgN with fine NO_3^- only constituting 10% of this total. The lifetime of fine nitrate (4.8 days) is shorter than that of coarse nitrate (7.0-7.1 days). The global lifetime of OXN (7.6-7.7 days) is longer than that of RDN (4.9-5.2 days), consistent with a total OXN burden (1.20 TgN) almost double that of RDN. The tropospheric burden of OXS is 0.78 TgS with a global lifetime of 5.6-5.9 days. The SO_4^{2-} burden is 0.63 TgS and its lifetime of 8.3-8.5 days is similar to that of NH_4^+, reflecting the close association between the two species in the atmosphere globally. It is notable that lifetimes of RDN, OXN, and OXS vary by a factor of 4 across different continental regions. East Asia has quite short lifetimes for RDN (2.9-3.0 days), OXN (3.9-4.5 days), and OXS (3.4-3.7 days), whereas the lifetimes in Rest of Asia and Africa are around twice as long, which is related to the regional differences in meteorological conditions and compositions of RDN, OXN, and OXS burdens.

The model confirms that the longer lifetimes of the secondary N_r and S_r species are consistent with their greater vertical transport, which surface measurements cannot reveal. In addition, whilst the gaseous precursor species have maximum concentrations at the surface, maximum concentrations of the aerosol species are at higher altitudes because of the time taken for their formation.

Comparison of the absolute emission and deposition fluxes of RDN and OXN in different world regionns show that East Asia and South Asia are characterised by larger RDN fluxes than OXN fluxes, while most other world regions exhibit larger OXN fluxes than RDN fluxes, which likely reflects greater increases in NH_3 emissions in the two regions.

Comparison of the difference between emission and deposition fluxes shows that South Asia region is the largest net exporter of RDN (2.21 TgN yr^{-1}, 29% of its annual emission), followed by Euro_Medi and Africa and other continental regions. Despite having the largest RDN emissions and depostion, East Asia has very small net export and is therefore largely responsible for its own RDN pollution. In contrast, Rest of world, which is mainly the ocean regions (as well as Southeast Asia which also contains a lot of marine area) receive more deposition of RDN than they emit.

For OXN, Africa is the largest net exporter of OXN at 22% (1.92 TgN yr^{-1}) of its emission, followed by South Asia. The Rest of world again receives substantial net import of OXN (11.2 TgN yr^{-1}) which is even higher than the 7.89 TgN yr^{-1} net import of RDN. Oxidation of NO_x to reservoir organic nitrate species such as PAN likely facilitates the long-distance transport of OXN from the continent to the ocean, whereas the short lifetime of NH_3 means less RDN is transported from its continental emissions regions. The large flux imbalances of OXN and RDN in these areas indicates the scale of anthropogenic N pollution to marine areas.

The two regions with the largest net export of OXS are South Asia (1.62 TgS yr^{-1}, equivalent to 37% of its emission) and Euro_Medi (1.52 TgS yr^{-1}, 27%). All other continental regions are either positive or zero exporters of OXS except for Southeast Asia which receives more OXS depostion than it emits. This is similar to the situation for RDN because away from major NO_x emission areas NH_4^+ is predominantly associated with SO_4^{2-}.

The three largest contributors to total N burden globally are NH_4^+, coarse NO_3^-, and 'Rest OXN' (mainly PAN). In South Asia, Rest of Asia, and Africa, coarse NO_3^- constitutes over half of OXN burden, attributable to an abundance of coarse sea-salt and dust particles in these regions. It is critical to account for contributions of coarse nitrate as it controls atmospheric nitrate burden and the size distribution of nitrate aerosol. Aerosol SO_4^{2-} is the predominant form of OXS in all regions.

As presented in this work, N_r and S_r species are abundant air pollutants impacting gas and particle concentrations and deposition globally. The chemical and meteorological linkages between emissions and N_r and S_r species concentrations are complex, and the detail can only be revealed by process-based atmospheric modelling as illustrated here, despite the uncertainties in emissions and model parameterisations.

Code and data availability

As described and referenced in Section 2 of this paper, this study used two open-source global models: the European Monitoring and Evaluation Programme Meteorological Synthesizing Centre -West atmospheric chemistry transport model (EMEP MSC-W, version 4.34, source code available at https://doi.org/10.5281/zenodo.3647990) and the Weather Research and Forecast meteorological model (WRF, version 4.2.2, www.wrf-model.org, https://github.com/wrf-model/WRF/releases/tag/v4.2.2). The model output presented in figures and tables in this paper and the corresponding Python scripts are available at https://doi.org/10.5281/zenodo.5912055.

Author contribution

MH, DS and MV conceptualised and supervised the study. MV and PW contributed to model development and set-up and provided modelling support. MV provided computing resource. YG contributed to study design, undertook all model simulations, formal data analyses, visualisation of the results and data curation, with discussion and refinement by all authors. The original draft of the paper was written by YG with contributions and editing by MH. All authors provided review comments and approval of the final version.

Competing interests

The authors declare that they have no conflict of interest.

Acknowledgments

Y. Ge gratefully acknowledges studentship funding from the University of Edinburgh and its School of Chemistry. This work was in part supported by the UK Natural Environment Research Council (NERC), including grant nos. NE/R016429/1 and NE/R000131/1 as part of the UK-SCAPE and SUNRISE programmes delivering UK National Capability, and the European Modelling and Evaluation Programme under the United Nations Economic Commission for Europe Convention on Long-range Transboundary Air Pollution.

References

Aas, W., Mortier, A., Bowersox, V., Cherian, R., Faluvegi, G., Fagerli, H., Hand, J., Klimont, Z., Galy-Lacaux, C., Lehmann, C. M. B., Myhre, C. L., Myhre, G., Olivié, D., Sato, K., Quaas, J., Rao, P. S. P., Schulz, M., Shindell, D., Skeie, R. B., Stein, A., Takemura, T., Tsyro, S., Vet, R., and Xu, X.: Global and regional trends of atmospheric sulfur, Scientific Reports, 9, 953, 10.1038/s41598-018-37304-0, 2019.

Ackerman, D., Millet, D. B., & Chen, X.: Global estimates of inorganic nitrogen deposition across four decades, Global Biogeochemical Cycles, 33, 100–107, https://doi.org/10.1029/2018GB005990, 2019.

Aksoyoglu, S., Jiang, J., Ciarelli, G., Baltensperger, U., and Prévôt, A. S. H.: Role of ammonia in European air quality with changing land and ship emissions between 1990 and 2030, Atmos. Chem. Phys., 20, 15665-15680, 10.5194/acp-20-15665-2020, 2020.

Alexander, B., Sherwen, T., Holmes, C. D., Fisher, J. A., Chen, Q., Evans, M. J., and Kasibhatla, P.: Global inorganic nitrate production mechanisms: comparison of a global model with nitrate isotope observations, Atmos. Chem. Phys., 20, 3859-3877, 10.5194/acp-20-3859-2020, 2020.

Aneja, V. P., Schlesinger, W. H., and Erisman, J. W.: Effects of Agriculture upon the Air Quality and Climate: Research, Policy, and Regulations, Environmental Science & Technology, 43, 4234-4240, 10.1021/es8024403, 2009.

Aneja, V. P., Schlesinger, W. H., Erisman, J. W., Behera, S. N., Sharma, M., and Battye, W.: Reactive nitrogen emissions from crop and livestock farming in India, Atmospheric Environment, 47, 92-103, https://doi.org/10.1016/j.atmosenv.2011.11.026, 2012.

Ansari, A. S., and Pandis, S. N.: Response of Inorganic PM to Precursor Concentrations, Environmental Science & Technology, 32, 2706-2714, 10.1021/es971130j, 1998.

Behera, S. N., Betha, R., Liu, P., and Balasubramanian, R.: A study of diurnal variations of PM2.5 acidity and related chemical species using a new thermodynamic equilibrium model, Science of The Total Environment, 452-453, 286-295, https://doi.org/10.1016/j.scitotenv.2013.02.062, 2013a.

Behera, S. N., Sharma, M., Aneja, V. P., and Balasubramanian, R.: Ammonia in the atmosphere: a review on emission sources, atmospheric chemistry and deposition on terrestrial bodies, Environmental Science and Pollution Research, 20, 8092-8131, https://doi.org/10.1007/s11356-013-2051-9, 2013b.

Bellouin, N., Rae, J., Jones, A., Johnson, C., Haywood, J., and Boucher, O.: Aerosol forcing in the Climate Model Intercomparison Project (CMIP5) simulations by HadGEM2-ES and the role of ammonium nitrate, Journal of Geophysical Research: Atmospheres, 116, https://doi.org/10.1029/2011JD016074, 2011.

Berge, E., and Jakobsen, H. A.: A regional scale multilayer model for the calculation of long-term transport and deposition of air pollution in Europe, Tellus B: Chemical and Physical Meteorology, 50, 205-223, 10.3402/tellusb.v50i3.16097, 1998.

Bergström, R., Denier van der Gon, H. A. C., Prévôt, A. S. H., Yttri, K. E., and Simpson, D.: Modelling of organic aerosols over Europe (2002-2007) using a volatility basis set (VBS) framework: application of different assumptions regarding the formation of secondary organic aerosol, Atmospheric Chemistry and Physics, 12, 8499-8527, 10.5194/acp-12-8499-2012, 2012.

Bergström, R., Hallquist, M., Simpson, D., Wildt, J., and Mentel, T. F.: Biotic stress: a significant contributor to organic aerosol in Europe?, Atmos. Chem. Phys., 14, 13643-13660, 10.5194/acp-14-13643-2014, 2014.

Deleted: ¶
¶
Page Break
¶

Deleted: 2013b.

Bian, H., Chin, M., Hauglustaine, D. A., Schulz, M., Myhre, G., Bauer, S. E., Lund, M. T., Karydis, V. A., Kucsera, T. L., Pan, X., Pozzer, A., Skeie, R. B., Steenrod, S. D., Sudo, K., Tsigaridis, K., Tsimpidi, A. P., and Tsyro, S. G.: Investigation of global particulate nitrate from the AeroCom phase III experiment, Atmospheric Chemistry and Physics, 17, 12911-12940, 10.5194/acp-17-12911-2017, 2017.

Bobbink, R., Hicks, K., Galloway, J., Spranger, T., Alkemade, R., Ashmore, M., Bustamante, M., Cinderby, S., Davidson, E., Dentener, F., Emmett, B., Erisman, J. W., Fenn, M., Gilliam, F., Nordin, A., Pardo, L., and De Vries, W.: Global assessment of nitrogen deposition effects on terrestrial plant diversity: a synthesis, Ecological Applications, 20, 30-59, https://doi.org/10.1890/08-1140.1, 2010.

Boreddy, S. K. R., Hegde, P., and Aswini, A. R.: Chemical Characteristics, Size Distributions, and Aerosol Liquid Water in Size-Resolved Coastal Urban Aerosols Allied with Distinct Air Masses over Tropical Peninsular India, ACS Earth and Space Chemistry, 5, 457-473, 10.1021/acsearthspacechem.0c00282, 2021.

Bray, C. D., Battye, W., Aneja, V. P., Tong, D. Q., Lee, P., and Tang, Y.: Ammonia emissions from biomass burning in the continental United States, Atmospheric Environment, 187, 50-61, https://doi.org/10.1016/j.atmosenv.2018.05.052, 2018.

Burnett, R., Chen, H., Szyszkowicz, M., Fann, N., Hubbell, B., Pope, C. A., Apte, J. S., Brauer, M., Cohen, A., Weichenthal, S., Coggins, J., Di, Q., Brunekreef, B., Frostad, J., Lim, S. S., Kan, H., Walker, K. D., Thurston, G. D., Hayes, R. B., Lim, C. C., Turner, M. C., Jerrett, M., Krewski, D., Gapstur, S. M., Diver, W. R., Ostro, B., Goldberg, D., Crouse, D. L., Martin, R. V., Peters, P., Pinault, L., Tjepkema, M., van Donkelaar, A., Villeneuve, P. J., Miller, A. B., Yin, P., Zhou, M., Wang, L., Janssen, N. A. H., Marra, M., Atkinson, R. W., Tsang, H., Quoc Thach, T., Cannon, J. B., Allen, R. T., Hart, J. E., Laden, F., Cesaroni, G., Forastiere, F., Weinmayr, G., Jaensch, A., Nagel, G., Concin, H., and Spadaro, J. V.: Global estimates of mortality associated with long-term exposure to outdoor fine particulate matter, Proceedings of the National Academy of Sciences, 115, 9592, 10.1073/pnas.1803222115, 2018.

Cohen, A. J., Brauer, M., Burnett, R., Anderson, H. R., Frostad, J., Estep, K., Balakrishnan, K., Brunekreef, B., Dandona, L., Dandona, R., Feigin, V., Freedman, G., Hubbell, B., Jobling, A., Kan, H., Knibbs, L., Liu, Y., Martin, R., Morawska, L., Pope, C. A., III, Shin, H., Straif, K., Shaddick, G., Thomas, M., van Dingenen, R., van Donkelaar, A., Vos, T., Murray, C. J. L., and Forouzanfar, M. H.: Estimates and 25-year trends of the global burden of disease attributable to ambient air pollution: an analysis of data from the Global Burden of Diseases Study 2015, The Lancet, 389, 1907-1918, 10.1016/S0140-6736(17)30505-6, 2017.

Crippa, M., Guizzardi, D., Muntean, M., Schaaf, E., Dentener, F., van Aardenne, J. A., Monni, S., Doering, U., Olivier, J. G. J., Pagliari, V., and Janssens-Maenhout, G.: Gridded emissions of air pollutants for the period 1970–2012 within EDGAR v4.3.2, Earth Syst. Sci. Data, 10, 1987-2013, 10.5194/essd-10-1987-2018, 2018.

Crippa, M., Solazzo, E., Huang, G., Guizzardi, D., Koffi, E., Muntean, M., Schieberle, C., Friedrich, R., and Janssens-Maenhout, G.: High resolution temporal profiles in the Emissions Database for Global Atmospheric Research, Scientific Data, 7, 121, 10.1038/s41597-020-0462-2, 2020.

Dammers, E., McLinden, C. A., Griffin, D., Shephard, M. W., Van Der Graaf, S., Lutsch, E., Schaap, M., Gainairu-Matz, Y., Fioletov, V., Van Damme, M., Whitburn, S., Clarisse, L., Cady-Pereira, K., Clerbaux, C., Coheur, P. F., and Erisman, J. W.: NH3 emissions from large point sources derived from CrIS and IASI satellite observations, Atmos. Chem. Phys., 19, 12261-12293, 10.5194/acp-19-12261-2019, 2019.

de Gouw, J. A., Parrish, D. D., Frost, G. J., and Trainer, M.: Reduced emissions of CO2, NOx, and SO2 from U.S. power plants owing to switch from coal to natural gas with combined cycle technology, Earth's Future, 2, 75-82, https://doi.org/10.1002/2013EF000196, 2014.

Dentener, F., Drevet, J., Lamarque, J. F., Bey, I., Eickhout, B., Fiore, A. M., Hauglustaine, D., Horowitz, L. W., Krol, M., Kulshrestha, U. C., Lawrence, M., Galy-Lacaux, C., Rast, S., Shindell, D., Stevenson, D., Van Noije, T., Atherton, C., Bell, N., Bergman, D., Butler, T., Cofala, J., Collins, B., Doherty, R., Ellingsen, K., Galloway, J., Gauss, M., Montanaro, V., Müller, J. F., Pitari, G., Rodriguez, J., Sanderson, M., Solmon, F., Strahan, S., Schultz, M., Sudo, K., Szopa, S., and Wild, O.: Nitrogen and sulfur deposition on regional and global scales: A multimodel evaluation, Global Biogeochemical Cycles, 20, https://doi.org/10.1029/2005GB002672, 2006.

Erisman, J. W., Domburg, N., de Vries, W., Kros, H., de Haan, B., and Sanders, K.: The Dutch N-cascade in the European perspective, Science in China Series C: Life Sciences, 48, 827-842, https://doi.org/10.1007/BF03187122, 2005.

Fagerli, H., Tsyro, S., Jonson, J. E., Nyíri, Á., Gauss, M., Simpson, D., Wind, P., Benetictow, A., Klein, H., Mortier, A., Aas, W., Hjellbrekke, A.-G., Solberg, S., Platt, S. M., Yttri, K. E., Tørseth, K., Gaisbauer, S., Mareckova, K., Matthews, B., Schindlbacher, S., Sosa, C., Tista, M., Ullrich, B., Wankmüller, R., Scheuschner, T., Bergström, R., Johanson, L., Jalkanen, J.-P., Metzger, S., van der Gon, H. A. C. D., Kuenen, J. J. P., Visschedijk, A. J. H., Barregård, L., Molnár, P., and Stockfelt, L.: Updates to the EMEP MSC-W model, 2018-2019, in: Transboundary particulate matter, photo-oxidants, acidifying and eutrophying components. EMEP Status Report 1/2019, METEOROLOGISK INSTITUTT Norwegian Meteorological Institute, Oslo, Norway15046109 (ISSN), 44, 2019.

Feng, Y., and Penner, J. E.: Global modeling of nitrate and ammonium: Interaction of aerosols and tropospheric chemistry, Journal of Geophysical Research: Atmospheres, 112, https://doi.org/10.1029/2005JD006404, 2007.

Fiddes, S. L., Woodhouse, M. T., Nicholls, Z., Lane, T. P., and Schofield, R.: Cloud, precipitation and radiation responses to large perturbations in global dimethyl sulfide, Atmos. Chem. Phys., 18, 10177-10198, 10.5194/acp-18-10177-2018, 2018.

Deleted: 2005.

Fioletov, V., McLinden, C. A., Griffin, D., Theys, N., Loyola, D. G., Hedelt, P., Krotkov, N. A., and Li, C.: Anthropogenic and volcanic point source SO2 emissions derived from TROPOMI on board Sentinel-5 Precursor: first results, Atmos. Chem. Phys., 20, 5591-5607, 10.5194/acp-20-5591-2020, 2020.

Fowler, D., Steadman, C. E., Stevenson, D., Coyle, M., Rees, R. M., Skiba, U. M., Sutton, M. A., Cape, J. N., Dore, A. J., Vieno, M., Simpson, D., Zaehle, S., Stocker, B. D., Rinaldi, M., Facchini, M. C., Flechard, C. R., Nemitz, E., Twigg, M., Erisman, J. W., Butterbach-Bahl, K., and Galloway, J. N.: Effects of global change during the 21st century on the nitrogen cycle, Atmospheric Chemistry and Physics, 15, 13849-13893, 10.5194/acp-15-13849-2015, 2015.

Fowler, D., Brimblecombe, P., Burrows, J., Heal, M. R., Grennfelt, P., Stevenson, D. S., Jowett, A., Nemitz, E., Coyle, M., Liu, X., Chang, Y., Fuller, G. W., Sutton, M. A., Klimont, Z., Unsworth, M. H., and Vieno, M.: A chronology of global air quality, Philosophical Transactions of the Royal Society A: Mathematical, Physical and Engineering Sciences, 378, 20190314, 10.1098/rsta.2019.0314, 2020.

Fowler, D., Coyle, M., Skiba, U., Sutton, M. A., Cape, J. N., Reis, S., Sheppard, L. J., Jenkins, A., Grizzetti, B., Galloway, J. N., Vitousek, P., Leach, A., Bouwman, A. F., Butterbach-Bahl, K., Dentener, F., Stevenson, D., Amann, M., and Voss, M.: The global nitrogen cycle in the twenty-first century, Philosophical Transactions of the Royal Society B: Biological Sciences, 368, 20130164, 10.1098/rstb.2013.0164, 2013.

Gallagher, M. W., Beswick, K. M., Duyzer, J., Westrate, H., Choularton, T. W., and Hummelshøj, P.: Measurements of aerosol fluxes to speulder forest using a micrometeorological technique, Atmospheric Environment, 31, 359-373, https://doi.org/10.1016/S1352-2310(96)00057-X, 1997.

Galloway, J. N., Townsend, A. R., Erisman, J. W., Bekunda, M., Cai, Z., Freney, J. R., Martinelli, L. A., Seitzinger, S. P., and Sutton, M. A.: Transformation of the Nitrogen Cycle: Recent Trends, Questions, and Potential Solutions, Science, 320, 889-892, 10.1126/science.1136674, 2008.

Ge, Y., Heal, M. R., Stevenson, D. S., Wind, P., and Vieno, M.: Evaluation of global EMEP MSC-W (rv4.34) WRF (v3.9.1.1) model surface concentrations and wet deposition of reactive N and S with measurements, Geosci. Model Dev., 14, 7021-7046, 10.5194/gmd-14-7021-2021, 2021.

Gu, B., Zhang, L., Van Dingenen, R., Vieno, M., Van Grinsven, H.J., Zhang, X., Zhang, S., Chen, Y., Wang, S., Ren, C. and Rao, S.: Abating ammonia is more cost-effective than nitrogen oxides for mitigating PM2. 5 air pollution, Science, 374(6568), 758-762, 10.1126/science.abf8623, 2021.

Hauglustaine, D. A., Balkanski, Y., and Schulz, M.: A global model simulation of present and future nitrate aerosols and their direct radiative forcing of climate, Atmospheric Chemistry and Physics, 14, 11031-11063, 10.5194/acp-14-11031-2014, 2014.

Hoesly, R. M., Smith, S. J., Feng, L., Klimont, Z., Janssens-Maenhout, G., Pitkanen, T., Seibert, J. J., Vu, L., Andres, R. J., Bolt, R. M., Bond, T. C., Dawidowski, L., Kholod, N., Kurokawa, J. I., Li, M., Liu, L., Lu, Z., Moura, M. C. P., O'Rourke, P. R., and Zhang, Q.: Historical (1750–2014) anthropogenic emissions of reactive gases and aerosols from the Community Emissions Data System (CEDS), Geosci. Model Dev., 11, 369-408, 10.5194/gmd-11-369-2018, 2018.

Hoffmann, E. H., Tilgner, A., Schrödner, R., Bräuer, P., Wolke, R., and Herrmann, H.: An advanced modeling study on the impacts and atmospheric implications of multiphase dimethyl sulfide chemistry, Proceedings of the National Academy of Sciences, 113, 11776, 10.1073/pnas.1606320113, 2016.

IPCC: Climate Change 2021: The Physical Science Basis. Contribution of Working Group I to the Sixth Assessment Report of the Intergovernmental Panel on Climate Change [Masson-Delmotte, V., P. Zhai, A. Pirani, S.L. Connors, C. Péan, S. Berger, N. Caud, Y. Chen, L. Goldfarb, M.I. Gomis, M. Huang, K. Leitzell, E. Lonnoy, J.B.R. Matthews, T.K. Maycock, T. Waterfield, O. Yelekçi, R. Yu, and B. Zhou (eds.)], Cambridge University Press, In Press, 2021.

Iturbide, M., Gutiérrez, J. M., Alves, L. M., Bedia, J., Cerezo-Mota, R., Cimadevilla, E., Cofiño, A. S., Di Luca, A., Faria, S. H., Gorodetskaya, I. V., Hauser, M., Herrera, S., Hennessy, K., Hewitt, H. T., Jones, R. G., Krakovska, S., Manzanas, R., Martínez-Castro, D., Narisma, G. T., Nurhati, I. S., Pinto, I., Seneviratne, S. I., van den Hurk, B., and Vera, C. S.: An update of IPCC climate reference regions for subcontinental analysis of climate model data: definition and aggregated datasets, Earth Syst. Sci. Data, 12, 2959-2970, 10.5194/essd-12-2959-2020, 2020.

Jackson, R. L., Gabric, A. J., Cropp, R., and Woodhouse, M. T.: Dimethylsulfide (DMS), marine biogenic aerosols and the ecophysiology of coral reefs, Biogeosciences, 17, 2181-2204, 10.5194/bg-17-2181-2020, 2020.

Jonson, J. E., Borken-Kleefeld, J., Simpson, D., Nyíri, A., Posch, M., and Heyes, C.: Impact of excess NO x emissions from diesel cars on air quality, public health and eutrophication in Europe, Environmental Research Letters, 12, 094017, 10.1088/1748-9326/aa8850, 2017.

Karl, M., Jonson, J. E., Uppstu, A., Aulinger, A., Prank, M., Sofiev, M., Jalkanen, J. P., Johansson, L., Quante, M., and Matthias, V.: Effects of ship emissions on air quality in the Baltic Sea region simulated with three different chemistry transport models, Atmos. Chem. Phys., 19, 7019-7053, 10.5194/acp-19-7019-2019, 2019.

Karydis, V. A., Tsimpidi, A. P., Pozzer, A., Astitha, M., and Lelieveld, J.: Effects of mineral dust on global atmospheric nitrate concentrations, Atmos. Chem. Phys., 16, 1491-1509, 10.5194/acp-16-1491-2016, 2016.

Khan, M. A. H., Lowe, D., Derwent, R. G., Foulds, A., Chhantyal-Pun, R., McFiggans, G., Orr-Ewing, A. J., Percival, C. J., and Shallcross, D. E.: Global and regional model simulations of atmospheric ammonia, Atmospheric Research, 234, 104702, https://doi.org/10.1016/j.atmosres.2019.104702, 2020.

Klimont, Z., Kupiainen, K., Heyes, C., Purohit, P., Cofala, J., Rafaj, P., Borken-Kleefeld, J., and Schöpp, W.: Global anthropogenic emissions of particulate matter including black carbon, Atmos. Chem. Phys., 17, 8681-8723, 10.5194/acp-17-8681-2017, 2017.

Kumar, A., and Sarin, M. M.: Atmospheric water-soluble constituents in fine and coarse mode aerosols from high-altitude site in western India: Long-range transport and seasonal variability, Atmospheric Environment, 44, 1245-1254, https://doi.org/10.1016/j.atmosenv.2009.12.035, 2010.

Kurokawa, J., and Ohara, T.: Long-term historical trends in air pollutant emissions in Asia: Regional Emission inventory in ASia (REAS) version 3, Atmos. Chem. Phys., 20, 12761-12793, 10.5194/acp-20-12761-2020, 2020.

Laakso, L., Grönholm, T., Rannik, Ü., Kosmale, M., Fiedler, V., Vehkamäki, H., and Kulmala, M.: Ultrafine particle scavenging coefficients calculated from 6 years field measurements, Atmospheric Environment, 37, 3605-3613, https://doi.org/10.1016/S1352-2310(03)00326-1, 2003.

Lamarque, J. F., Dentener, F., McConnell, J., Ro, C. U., Shaw, M., Vet, R., Bergmann, D., Cameron-Smith, P., Dalsoren, S., Doherty, R., Faluvegi, G., Ghan, S. J., Josse, B., Lee, Y. H., MacKenzie, I. A., Plummer, D., Shindell, D. T., Skeie, R. B., Stevenson, D. S., Strode, S., Zeng, G., Curran, M., Dahl-Jensen, D., Das, S., Fritzsche, D., and Nolan, M.: Multi-model mean nitrogen and sulfur deposition from the Atmospheric Chemistry and Climate Model Intercomparison Project (ACCMIP): evaluation of historical and projected future changes, Atmos. Chem. Phys., 13, 7997-8018, 10.5194/acp-13-7997-2013, 2013.

Lamaud, E., Brunet, Y., Labatut, A., Lopez, A., Fontan, J., and Druilhet, A.: The Landes experiment: Biosphere-atmosphere exchanges of ozone and aerosol particles above a pine forest, Journal of Geophysical Research: Atmospheres, 99, 16511-16521, https://doi.org/10.1029/94JD00668, 1994.

Lee, Y. N., Springston, S., Jayne, J., Wang, J., Hubbe, J., Senum, G., Kleinman, L., and Daum, P. H.: Chemical composition and sources of coastal marine aerosol particles during the 2008 VOCALS-REx campaign, Atmos. Chem. Phys., 14, 5057-5072, 10.5194/acp-14-5057-2014, 2014.

Lelieveld, J., ., Evans, J. S., Fnais, M., ., Giannadaki, D., ., and Pozzer, A., . The contribution of outdoor air pollution sources to premature mortality on a global scale, Nature, 525, 367-371, https://doi.org/10.1038/nature15371, 2015.

Liu, M., Huang, X., Song, Y., Xu, T., Wang, S., Wu, Z., Hu, M., Zhang, L., Zhang, Q., Pan, Y., Liu, X., and Zhu, T.: Rapid SO2 emission reductions significantly increase tropospheric ammonia concentrations over the North China Plain, Atmos. Chem. Phys., 18, 17933-17943, 10.5194/acp-18-17933-2018, 2018.

Liu, M., and Matsui, H.: Aerosol radiative forcings induced by substantial changes in anthropogenic emissions in China from 2008 to 2016, Atmos. Chem. Phys., 21, 5965-5982, 10.5194/acp-21-5965-2021, 2021.

Marandino, C. A., Tegtmeier, S., Krüger, K., Zindler, C., Atlas, E. L., Moore, F., and Bange, H. W.: Dimethylsulphide (DMS) emissions from the western Pacific Ocean: a potential marine source for stratospheric sulfur?, Atmos. Chem. Phys., 13, 8427-8437, 10.5194/acp-13-8427-2013, 2013.

McFiggans, G., Mentel, T. F., Wildt, J., Pullinen, I., Kang, S., Kleist, E., Schmitt, S., Springer, M., Tillmann, R., Wu, C., Zhao, D., Hallquist, M., Faxon, C., Le Breton, M., Hallquist, Å. M., Simpson, D., Bergström, R., Jenkin, M. E., Ehn, M., Thornton, J. A., Alfarra, M. R., Bannan, T. J., Percival, C. J., Priestley, M., Topping, D., and Kiendler-Scharr, A.: Secondary organic aerosol reduced by mixture of atmospheric vapours, Nature, 565, 587-593, 10.1038/s41586-018-0871-y, 2019.

McHale, M. R., Ludtke, A. S., Wetherbee, G. A., Burns, D. A., Nilles, M. A., and Finkelstein, J. S.: Trends in precipitation chemistry across the U.S. 1985–2017: Quantifying the benefits from 30 years of Clean Air Act amendment regulation, Atmospheric Environment, 247, 118219, https://doi.org/10.1016/j.atmosenv.2021.118219, 2021.

Metzger, S., Dentener, F., Krol, M., Jeuken, A., and Lelieveld, J.: Gas/aerosol partitioning 2. Global modeling results, Journal of Geophysical Research: Atmospheres, 107, ACH 17-11-ACH 17-23, https://doi.org/10.1029/2001JD001103, 2002a.

Metzger, S., Dentener, F., Pandis, S., and Lelieveld, J.: Gas/aerosol partitioning: 1. A computationally efficient model, Journal of Geophysical Research: Atmospheres, 107, ACH 16-11-ACH 16-24, https://doi.org/10.1029/2001JD001102, 2002b.

Metzger, S., Steil, B., Xu, L., Penner, J. E., and Lelieveld, J.: New representation of water activity based on a single solute specific constant to parameterize the hygroscopic growth of aerosols in atmospheric models, Atmos. Chem. Phys., 12, 5429-5446, 10.5194/acp-12-5429-2012, 2012.

Deleted: 2015.

Metzger, S., Steil, B., Abdelkader, M., Klingmüller, K., Xu, L., Penner, J. E., Fountoukis, C., Nenes, A., and Lelieveld, J.: Aerosol water parameterisation: a single parameter framework, Atmos. Chem. Phys., 16, 7213-7237, 10.5194/acp-16-7213-2016, 2016.

Metzger, S., Abdelkader, M., Steil, B., and Klingmüller, K.: Aerosol water parameterization: long-term evaluation and importance for climate studies, Atmos. Chem. Phys., 18, 16747-16774, 10.5194/acp-18-16747-2018, 2018.

Myhre, G., Aas, W., Cherian, R., Collins, W., Faluvegi, G., Flanner, M., Forster, P., Hodnebrog, Ø., Klimont, Z., Lund, M. T., Mülmenstädt, J., Lund Myhre, C., Olivié, D., Prather, M., Quaas, J., Samset, B. H., Schnell, J. L., Schulz, M., Shindell, D., Skeie, R. B., Takemura, T., and Tsyro, S.: Multi-model simulations of aerosol and ozone radiative forcing due to anthropogenic emission changes during the period 1990–2015, Atmos. Chem. Phys., 17, 2709-2720, 10.5194/acp-17-2709-2017, 2017.

Nemitz, E., Sutton, M. A., Wyers, G. P., Otjes, R. P., Mennen, M. G., van Putten, E. M., and Gallagher, M. W.: Gas-particle interactions above a Dutch heathland: II. Concentrations and surface exchange fluxes of atmospheric particles, Atmos. Chem. Phys., 4, 1007-1024, 10.5194/acp-4-1007-2004, 2004.

Nenes, A., Pandis, S. N., Weber, R. J., and Russell, A.: Aerosol pH and liquid water content determine when particulate matter is sensitive to ammonia and nitrate availability, Atmos. Chem. Phys., 20, 3249-3258, 10.5194/acp-20-3249-2020, 2020.

Pandey, A., Sadavarte, P., Rao, A. B., and Venkataraman, C.: Trends in multi-pollutant emissions from a technology-linked inventory for India: II. Residential, agricultural and informal industry sectors, Atmospheric Environment, 99, 341-352, https://doi.org/10.1016/j.atmosenv.2014.09.080, 2014.

Park, R. J., Jacob, D. J., Field, B. D., Yantosca, R. M., and Chin, M.: Natural and transboundary pollution influences on sulfate-nitrate-ammonium aerosols in the United States: Implications for policy, Journal of Geophysical Research: Atmospheres, 109, https://doi.org/10.1029/2003JD004473, 2004.

Petroff, A., Mailliat, A., Amielh, M., and Anselmet, F.: Aerosol dry deposition on vegetative canopies. Part I: Review of present knowledge, Atmospheric Environment, 42, 3625-3653, https://doi.org/10.1016/j.atmosenv.2007.09.043, 2008a.

Petroff, A., Mailliat, A., Amielh, M., and Anselmet, F.: Aerosol dry deposition on vegetative canopies. Part II: A new modelling approach and applications, Atmospheric Environment, 42, 3654-3683, https://doi.org/10.1016/j.atmosenv.2007.12.060, 2008b.

Pescott, O. L., Simkin, J. M., August, T. A., Randle, Z., Dore, A. J., and Botham, M. S.: Air pollution and its effects on lichens, bryophytes, and lichen-feeding Lepidoptera: review and evidence from biological records, Biological Journal of the Linnean Society, 115, 611-635, 10.1111/bij.12541, 2015.

Pommier, M., Fagerli, H., Schulz, M., Valdebenito, A., Kranenburg, R., and Schaap, M.: Prediction of source contributions to urban background PM10 concentrations in European cities: a case study for an episode in December 2016 using EMEP/MSC-W rv4.15 and LOTOS-EUROS v2.0 – Part 1: The country contributions, Geoscientific Model Development, 13, 1787-1807, 10.5194/gmd-13-1787-2020, 2020.

Sadavarte, P., and Venkataraman, C.: Trends in multi-pollutant emissions from a technology-linked inventory for India: I. Industry and transport sectors, Atmospheric Environment, 99, 353-364, https://doi.org/10.1016/j.atmosenv.2014.09.081, 2014.

Saha, S., Moorthi, S., Pan, H.-L., Wu, X., Wang, J., Nadiga, S., Tripp, P., Kistler, R., Woollen, J., Behringer, D., Liu, H., Stokes, D., Grumbine, R., Gayno, G., Wang, J., Hou, Y.-T., Chuang, H.-y., Juang, H.-M. H., Sela, J., Iredell, M., Treadon, R., Kleist, D., Van Delst, P., Keyser, D., Derber, J., Ek, M., Meng, J., Wei, H., Yang, R., Lord, S., van den Dool, H., Kumar, A., Wang, W., Long, C., Chelliah, M., Xue, Y., Huang, B., Schemm, J.-K., Ebisuzaki, W., Lin, R., Xie, P., Chen, M., Zhou, S., Higgins, W., Zou, C.-Z., Liu, Q., Chen, Y., Han, Y., Cucurull, L., Reynolds, R. W., Rutledge, G., and Goldberg, M.: The NCEP Climate Forecast System Reanalysis, Bulletin of the American Meteorological Society, 91, 1015-1058, 10.1175/2010BAMS3001.1, 2010.

Schobesberger, S., Junninen, H., Bianchi, F., Lönn, G., Ehn, M., Lehtipalo, K., Dommen, J., Ehrhart, S., Ortega, I. K., Franchin, A., Nieminen, T., Riccobono, F., Hutterli, M., Duplissy, J., Almeida, J., Amorim, A., Breitenlechner, M., Downard, A. J., Dunne, E. M., Flagan, R. C., Kajos, M., Keskinen, H., Kirkby, J., Kupc, A., Kürten, A., Kurtén, T., Laaksonen, A., Mathot, S., Onnela, A., Praplan, A. P., Rondo, L., Santos, F. D., Schallhart, S., Schnitzhofer, R., Sipilä, M., Tomé, A., Tsagkogeorgas, G., Vehkamäki, H., Wimmer, D., Baltensperger, U., Carslaw, K. S., Curtius, J., Hansel, A., Petäjä, T., Kulmala, M., Donahue, N. M., and Worsnop, D. R.: Molecular understanding of atmospheric particle formation from sulfuric acid and large oxidized organic molecules, Proceedings of the National Academy of Sciences, 110, 17223, 10.1073/pnas.1306973110, 2013.

Schwier, A. N., Sellegri, K., Mas, S., Charrière, B., Pey, J., Rose, C., Temime-Roussel, B., Jaffrezo, J. L., Parin, D., Picard, D., Ribeiro, M., Roberts, G., Sempéré, R., Marchand, N., and D'Anna, B.: Primary marine aerosol physical flux and chemical composition during a nutrient enrichment experiment in mesocosms in the Mediterranean Sea, Atmos. Chem. Phys., 17, 14645-14660, 10.5194/acp-17-14645-2017, 2017.

Simpson, D., Benedictow, A., Berge, H., Bergström, R., Emberson, L. D., Fagerli, H., Flechard, C. R., Hayman, G. D., Gauss, M., Jonson, J. E., Jenkin, M. E., Nyíri, A., Richter, C., Semeena, V. S., Tsyro, S., Tuovinen, J. P., Valdebenito, Á., and Wind, P.: The EMEP MSC-W chemical transport model – technical description, Atmos. Chem. Phys., 12, 7825-7865, 10.5194/acp-12-7825-2012, 2012.

Simpson, D., Bergström, R., Briolat, A., Imhof, H., Johansson, J., Priestley, M., and Valdebenito, A.: GenChem v1.0 – a chemical pre-processing and testing system for atmospheric modelling, Geosci. Model Dev., 13, 6447-6465, 10.5194/gmd-13-6447-2020, 2020.

Simpson, D., Bergström, R., Imhof, H., Wind, P.: Updates to the EMEP/MSC-W model, 2016--2017, in: Transboundary particulate matter, photo-oxidants, acidifying and eutrophying components. Status Report 1/2017, The Norwegian Meteorological Institute, Oslo, Norway, www.emep.int, 115-122, 2017.

Sun, J., Fu, J. S., Lynch, J. A., Huang, K., and Gao, Y.: Climate-driven exceedance of total (wet + dry) nitrogen (N) + sulfur (S) deposition to forest soil over the conterminous U.S, Earth's Future, 5, 560-576, https://doi.org/10.1002/2017EF000588, 2017.

Sutton, M. A., Mason, K. E., Sheppard, L. J., Sverdrup, H., Haeuber, R., and Hicks, W. K.: Nitrogen Deposition, Critical Loads and Biodiversity, Springer, Dordrecht, 535 pp., 2014.

Sutton, M. A., Reis, S., Riddick, S. N., Dragosits, U., Nemitz, E., Theobald, M. R., Tang, Y. S., Braban, C. F., Vieno, M., Dore, A. J., Mitchell, R. F., Wanless, S., Daunt, F., Fowler, D., Blackall, T. D., Milford, C., Flechard, C. R., Loubet, B., Massad, R., Cellier, P., Personne, E., Coheur, P. F., Clarisse, L., Van Damme, M., Ngadi, Y., Clerbaux, C., Skjøth, C. A., Geels, C., Hertel, O., Wichink Kruit, R. J., Pinder, R. W., Bash, J. O., Walker, J. T., Simpson, D., Horváth, L., Misselbrook, T. H., Bleeker, A., Dentener, F., and de Vries, W.: Towards a climate-dependent paradigm of ammonia emission and deposition, Philosophical Transactions of the Royal Society B: Biological Sciences, 368, 20130166, 10.1098/rstb.2013.0166, 2013.

Sutton, M. A., van Dijk, N., Levy, P. E., Jones, M. R., Leith, I. D., Sheppard, L. J., Leeson, S., Sim Tang, Y., Stephens, A., Braban, C. F., Dragosits, U., Howard, C. M., Vieno, M., Fowler, D., Corbett, P., Naikoo, M. I., Munzi, S., Ellis, C. J., Chatterjee, S., Steadman, C. E., Móring, A., and Wolseley, P. A.: Alkaline air: changing perspectives on nitrogen and air pollution in an ammonia-rich world, Philosophical Transactions of the Royal Society A: Mathematical, Physical and Engineering Sciences, 378, 20190315, 10.1098/rsta.2019.0315, 2020.

Tan, J., Fu, J. S., Dentener, F., Sun, J., Emmons, L., Tilmes, S., Sudo, K., Flemming, J., Jonson, J. E., Gravel, S., Bian, H., Davila, Y., Henze, D. K., Lund, M. T., Kucsera, T., Takemura, T., and Keating, T.: Multi-model study of HTAP II on sulfur and nitrogen deposition, Atmos. Chem. Phys., 18, 6847-6866, 10.5194/acp-18-6847-2018, 2018.

Thornhill, G. D., Collins, W. J., Kramer, R. J., Olivié, D., Skeie, R. B., O'Connor, F. M., Abraham, N. L., Checa-Garcia, R., Bauer, S. E., Deushi, M., Emmons, L. K., Forster, P. M., Horowitz, L. W., Johnson, B., Keeble, J., Lamarque, J. F., Michou, M., Mills, M. J., Mulcahy, J. P., Myhre, G., Nabat, P., Naik, V., Oshima, N., Schulz, M., Smith, C. J., Takemura, T., Tilmes, S., Wu, T., Zeng, G., and Zhang, J.: Effective radiative forcing from emissions of reactive gases and aerosols – a multi-model comparison, Atmos. Chem. Phys., 21, 853-874, 10.5194/acp-21-853-2021, 2021.

Tsyro, S., Aas, W., Soares, J., Sofiev, M., Berge, H., and Spindler, G.: Modelling of sea salt concentrations over Europe: key uncertainties and comparison with observations, Atmos. Chem. Phys., 11, 10367-10388, 10.5194/acp-11-10367-2011, 2011.

UNECE: Assessment Report on Ammonia – 2020, available at https://unece.org/fileadmin/DAM/env/documents/2020/AIR/WGSR/Final_Assessment_Report_on_Ammonia_v2_20201126_b.pdf, Draft November 2020.

Van Herk, C. M., Mathijssen-Spiekman, E. A. M., and de Zwart, D.: Long distance nitrogen air pollution effects on lichens in Europe, The Lichenologist, 35, 347-359, 10.1016/S0024-2829(03)00036-7, 2003.

Vieno, M., Dore, A. J., Stevenson, D. S., Doherty, R., Heal, M. R., Reis, S., Hallsworth, S., Tarrason, L., Wind, P., Fowler, D., Simpson, D., and Sutton, M. A.: Modelling surface ozone during the 2003 heat-wave in the UK, Atmos. Chem. Phys., 10, 7963–7978, https://doi.org/10.5194/acp-10-7963-2010, 2010.

Vieno, M., Heal, M. R., Hallsworth, S., Famulari, D., Doherty, R. M., Dore, A. J., Tang, Y. S., Braban, C. F., Leaver, D., Sutton, M. A., and Reis, S.: The role of long-range transport and domestic emissions in determining atmospheric secondary inorganic particle concentrations across the UK, Atmos. Chem. Phys., 14, 8435–8447, https://doi.org/10.5194/acp-14-8435-2014, 2014.

Vieno, M., Heal, M. R., Williams, M. L., Carnell, E. J., Nemitz, E., Stedman, J. R., and Reis, S.: The sensitivities of emissions reductions for the mitigation of UK PM2.5, Atmos. Chem. Phys., 16, 265–276, https://doi.org/10.5194/acp-16-265-2016, 2016.

Wang, C., Yin, S., Bai, L., Zhang, X., Gu, X., Zhang, H., Lu, Q., and Zhang, R.: High-resolution ammonia emission inventories with comprehensive analysis and evaluation in Henan, China, 2006–2016, Atmospheric Environment, 193, 11-23, https://doi.org/10.1016/j.atmosenv.2018.08.063, 2018.

Deleted: and

Deleted: –

Deleted: Atmospheric Chemistry and Physics,

Westervelt, D. M., Conley, A. J., Fiore, A. M., Lamarque, J. F., Shindell, D., Previdi, M., Faluvegi, G., Correa, G., and Horowitz, L. W.: Multimodel precipitation responses to removal of U.S. sulfur dioxide emissions, Journal of Geophysical Research: Atmospheres, 122, 5024-5038, https://doi.org/10.1002/2017JD026756, 2017.

Westervelt, D. M., Fiore, A. M., Baublitz, C. B., and Correa, G.: Impact of regional Northern Hemisphere mid-latitude anthropogenic sulfur dioxide emissions on local and remote tropospheric oxidants, Atmos. Chem. Phys., 21, 6799-6810, 10.5194/acp-21-6799-2021, 2021.

Whitburn, S., Van Damme, M., Kaiser, J. W., van der Werf, G. R., Turquety, S., Hurtmans, D., Clarisse, L., Clerbaux, C., and Coheur, P. F.: Ammonia emissions in tropical biomass burning regions: Comparison between satellite-derived emissions and bottom-up fire inventories, Atmospheric Environment, 121, 42-54, https://doi.org/10.1016/j.atmosenv.2015.03.015, 2015.

Xu, L., and Penner, J. E.: Global simulations of nitrate and ammonium aerosols and their radiative effects, Atmos. Chem. Phys., 12, 9479-9504, 10.5194/acp-12-9479-2012, 2012.

Xue, J., Lau, A. K. H., and Yu, J. Z.: A study of acidity on PM2.5 in Hong Kong using online ionic chemical composition measurements, Atmospheric Environment, 45, 7081-7088, https://doi.org/10.1016/j.atmosenv.2011.09.040, 2011.

Zhu, L., Henze, D., Bash, J., Jeong, G. R., Cady-Pereira, K., Shephard, M., Luo, M., Paulot, F., and Capps, S.: Global evaluation of ammonia bidirectional exchange and livestock diurnal variation schemes, Atmos. Chem. Phys., 15, 12823-12843, 10.5194/acp-15-12823-2015, 2015.